Fractional Ca^{2+} Currents through TRP and TRPL Channels in *Drosophila* Photoreceptors

Brian Chu,[†] Marten Postma,[‡*] and Roger C. Hardie[†*]
[†]Department of Physiology, Development and Neuroscience, Cambridge University, Cambridge, UK; and [‡]Section of Molecular Cytology, Swammerdam Institute for Life Sciences, University of Amsterdam, Amsterdam, The Netherlands

ABSTRACT Light responses in *Drosophila* photoreceptors are mediated by two Ca^{2+} permeable cation channels, transient receptor potential (TRP) and TRP-like (TRPL). Although Ca^{2+} influx via these channels is critical for amplification, inactivation, and light adaptation, the fractional contribution of Ca^{2+} to the currents (P_f) has not been measured. We describe a slow (τ ~ 350 ms) tail current in voltage-clamped light responses and show that it is mediated by electrogenic Na^+/Ca^{2+} exchange. Assuming a 3Na:1Ca stoichiometry, we derive empirical estimates of P_f by comparing the charge integrals of the exchanger and light-induced currents. For TRPL channels, P_f was ~17% as predicted by Goldman-Hodgkin-Katz (GHK) theory. P_f for TRP (29%) and wild-type flies (26%) was higher, but lower than the GHK prediction (45% and 42%). As predicted by GHK theory, P_f for both channels increased with extracellular [Ca^{2+}], and was largely independent of voltage between –100 and –30 mV. A model incorporating intra- and extracellular geometry, ion permeation, diffusion, extrusion, and buffering suggested that the deviation from GHK predictions was largely accounted for by extracellular ionic depletion during the light-induced currents, and the time course of the Na^+/Ca^{2+} exchange current could be used to obtain estimates of cellular Ca^{2+} buffering capacities.

INTRODUCTION

Light activation of fly photoreceptors leads to the opening of two classes of Ca^{2+} permeable cation channels, transient receptor potential (TRP) and transient receptor potential-like (TRPL), via a G-protein-coupled PLC signaling cascade (1,2–4). Both the channels and upstream signaling elements are localized within the rhabdomere, a rod-like stack of ~35,000 tightly packed microvilli, 1–2 μm in length and 60 nm in diameter. The Ca^{2+} influx associated with the light response accounts for virtually all of the light-induced Ca^{2+} rise in the photoreceptor (5–7) and is proposed to transiently reach near-millimolar levels within individual microvilli in response to single-photon absorptions (8,9). The Ca^{2+} influx is critical for response amplification, inactivation, and light adaptation, and mediates sequential positive and negative feedback via multiple molecular targets (10–12). These include the light-sensitive channels, which are both positively and negatively regulated by Ca^{2+} (12–14), and PLC (12,15) and metarhodopsin (16), which are both inhibited by Ca^{2+} influx. The resulting light response in flies represents the fastest known G-protein-coupled signaling cascade and has a huge dynamic range, from single photon responses (quantum bumps) to full daylight (17,18). This performance, which outstrips that of any vertebrate photoreceptor, has inspired a number of computational models that attempt to account for the light response in terms of the underlying molecular mechanisms (4,19–21).

A key parameter in such models is the amount of Ca^{2+} that enters into individual microvilli via the light-sensitive channels. This requires knowledge of the fraction of light-induced current (LIC) that is carried by Ca^{2+}, i.e., the fractional Ca^{2+} current, P_f (22). P_f has never been directly measured, and previous estimates have relied upon theoretical values calculated from relative ionic permeabilities using the Goldman-Hodgkin-Katz (GHK) current equation (Eq. 1). However, it is questionable whether the independent mobility of ions, a central assumption of GHK theory (23), holds true for the light-sensitive channels, which show complex permeation and divalent ion block (24–26). In addition, the LIC can be so large that there may be significant changes in ionic gradients during the response.

For technical reasons, standard approaches for measuring P_f (22) are impractical for fly photoreceptors. In this study, we developed a novel (to our knowledge) approach that exploits the native electrogenic Na^+/Ca^{2+} exchanger (CalX), which extrudes 1 Ca^{2+} ion for the entry of 3 Na^+ ions (27–29). Using whole-cell recordings, we observed a distinct slow aftercurrent in response to bright flashes, which we attribute to electrogenic Na^+/Ca^{2+} exchange. Under the assumption that this tail current represents the extrusion of Ca^{2+} that entered through the TRP and/or TRPL channels, we estimated empirical P_f values for TRP and/or TRPL channels from the ratio between the charge carried by the LIC and the exchanger current. Empirical P_f values for TRPL channels closely matched the simple GHK prediction (P_f ~17%) but were somewhat below the prediction for TRP channels (empirical P_f ~29%, compared with ~45% for GHK-P_f). A detailed model incorporating intra- and extracellular geometry, ion permeation, diffusion, extrusion, and buffering suggested that the deviation from the GHK prediction could be largely accounted for by extracellular ionic depletion during the large LIC, and the time course of the Na^+/Ca^{2+} exchange tail current could

Submitted January 21, 2013, and accepted for publication March 25, 2013.
*Correspondence: rch14@cam.ac.uk or M.Postma@uva.nl
Editor: Godfrey Smith.

0006-3495/13/05/1905/12 $2.00
http://dx.doi.org/10.1016/j.bpj.2013.03.047

be used to obtain estimates of cellular Ca^{2+} buffering capacities.

MATERIALS AND METHODS

Flies

Flies (*Drosophila melanogaster*) were reared at 25°C in the dark. The wild-type (WT) strain was Oregon. The mutants used included trp^{343} and $trpl^{302}$, null alleles of TRP and TRPL channels, respectively (30,31); $calx^{A}$, a loss-of-function mutation of the Na^+/Ca^{2+} exchanger (29); and *dSK*, a deletion of the *dSK* gene encoding a small-conductance, Ca^{2+}-activated K channel (32).

Whole-cell electrophysiology

Dissociated ommatidia were prepared from newly eclosed flies as described previously (33) and transferred to a recording chamber on an inverted Nikon Diaphot microscope (Nikon, Kingston-upon-Thames, U.K.). The standard bath contained (in mM) 120 NaCl, 5 KCl, 10 *N*-Tris-(hydroxymethyl)-methyl-2-amino-ethanesulphonic acid, 4 $MgCl_2$, 1.5 $CaCl_2$, 25 proline and 5 alanine, pH 7.15. The intracellular pipette solution was 110 Cs gluconate, 15 TEACl, 10 *N*-Tris-(hydroxymethyl)-methyl-2-amino-ethanesulphonic acid 4 Mg-ATP, 2 $MgCl_2$, 1 NAD, and 0.4 Na-GTP, pH 7.15 (adjusted with CsOH). Chemicals were obtained from Sigma-Aldrich (Gillingham, U.K.). Whole-cell voltage-clamp recordings were made at room temperature (20°C ± 1°C) at –70 mV unless otherwise stated (including correction for a –10 mV junction potential) using electrodes of resistance ~10–15 MΩ. Series resistance values were generally <30 MΩ and were compensated to >80%. Data were collected and analyzed using an Axopatch 2D amplifier and pCLAMP9 software (Molecular Devices, Union City, CA). Photoreceptors were stimulated via green-light-emitting diodes, and intensities were calibrated in terms of effectively absorbed photons by counting quantum bumps at low intensities.

Measurement of P_f

Assuming that Ca^{2+} ions that enter through light-activated channels are all extruded by the CalX exchanger, the fractional Ca^{2+} current (P_f) can be calculated from the charge ratio of the total LIC and the extruded Ca^{2+}. The onset of the Na^+/Ca^{2+} exchange current is masked by the much larger LIC, and we estimated this hidden component by extrapolating an exponential fit back to the time of the peak response (Fig. 1 B). This would have introduced an error of <5% compared with more sophisticated modeling of the CalX current based on the overall response waveform (Fig. S2 in the Supporting Material). The charge integral of the LIC was calculated by subtracting the estimated CalX charge integral from the charge integral of the entire response. Assuming a stoichiometry of 3 Na^+ to 1 Ca^{2+}, the charge integral of the tail current was multiplied by two to correct for the divalency of the extruded Ca^{2+} ions and divided by the LIC charge integral to obtain an empirical estimate of P_f.

Theoretical fractional currents

In the first instance, we compared the experimentally measured fractional Ca^{2+} current (P_f) values with theoretical predictions based on ionic permeability ratios using the GHK current equation (Eq. 1), which specifies the current (I) across the membrane carried by ion species S with charge z_s:

$$I_S = P_S z_S^2 \frac{E_m F^2}{RT} \frac{[S]_i - [S]_o \exp(-z_s E_m F/RT)}{1 - \exp(-z_s E_m F/RT)} \quad (1)$$

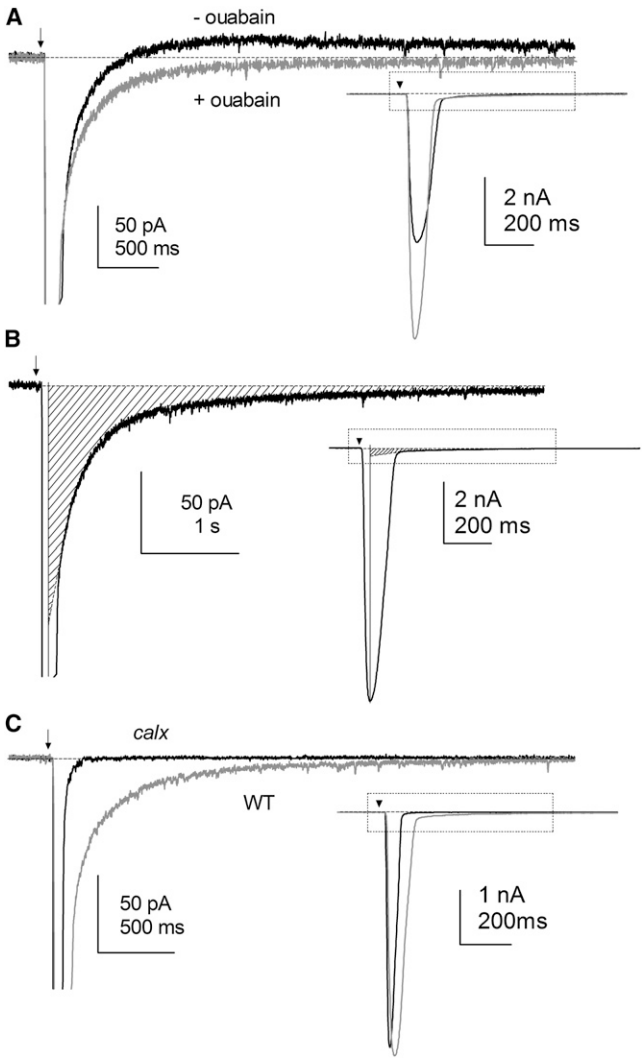

FIGURE 1 Light-induced tail currents in *Drosophila* photoreceptors. (*A*) Whole-cell voltage-clamped recording from WT photoreceptor at −70 mV to bright flashes (5 ms, ~17,500 effective photons; *arrow*) in the presence (*gray* trace) and absence (*black* trace) of 100 μM ouabain in normal bath (1.5 mM Ca^{2+}). A small, slow, outward aftercurrent (maximally ~30 pA) due to electrogenic Na^+/K^+ ATPase, was eliminated by ouabain. Inset: scaled to show entire response. (*B*) Measurement of the Na^+/Ca^{2+} exchange tail current in presence of ouabain (recording from the *trpl* mutant). The onset of the tail current is masked by the much larger LIC; this hidden component was estimated by extrapolating an exponential back to the time of the peak response and the charge integral measured (*shaded area*). (*C*) Responses to flashes containing ~17,500 photons in WT and *calx* mutants in the presence of ouabain. The conspicuous tail current was absent in *calx* mutants.

where E_m denotes membrane voltage, R is the gas constant, T is temperature (K), and F is the Faraday constant. $[S]_i$ and $[S]_o$ respectively denote the intra- and extracellular concentrations of ion S, and P_s is its permeability. $[Ca^{2+}]_i$ was taken as 160 nM in dark-adapted photoreceptors (7), other values from the experimental solutions. Under physiological conditions, the total LIC is carried by four main cations (Na^+, K^+, Ca^{2+}, and Mg^{2+}) (14):

$$I_{total} = I_{Na} + I_K + I_{Ca} + I_{Mg} \quad (2)$$

Table 1 shows theoretical P_f values for the WT and *trp* and *trpl* mutants in a standard bath based on Eq. 1 using published ionic permeability ratios (14,26).

RESULTS

Na^+/Ca^{2+} exchange tail current

In whole-cell, voltage-clamped recordings from *Drosophila* photoreceptors, the responses to brief, intense flashes exhibit a distinct slow, inward tail current of ~100 pA (Fig. 1 *A*). Because the photoreceptors express high densities of an NCX electrogenic Na^+/Ca^{2+} exchanger, encoded by *calx* (28,29,34,35), we suspected that this tail current was an electrogenic Na^+/Ca^{2+} exchange current. A slowly inactivating depolarizing afterpotential with similar kinetics was previously reported in intracellular recordings from larger flies and also attributed to electrogenic Na^+/Ca^{2+} exchange (36,37).

In principle, the charge integral of such an exchange current can be used to estimate the amount of Ca^{2+} that is extruded from the cell; however, this assumes that there are no other ionic fluxes that might otherwise overlap the putative Na^+/Ca^{2+} exchange current. In fact, the tail current of the photoresponse is normally also associated with a small outward component that develops slowly and decays over several seconds. This current is attributable to a Na^+/K^+ ATPase (4,37,38) and was completely abolished by 100 μM ouabain (Fig. 1), which we therefore used in all quantitative experiments.

To test more rigorously whether the tail current represents CalX exchanger activity, we examined light responses in $calx^A$ loss-of-function mutants. As previously reported (29), photoreceptors from $calx^A$ mutants have reduced sensitivity to light and rapid response kinetics resulting from elevated resting cytosolic Ca^{2+} due to the failure of Ca^{2+} extrusion via CalX. Importantly, the slow inward tail current was absent in $calx^A$ mutants, strongly supporting its identification as the exchanger current (Fig. 1 *C*).

An alternative explanation for the tail current could be persistent residual activation of the light-sensitive channels. If this were the case, it should show the characteristic pronounced outward rectification and reversal potential (E_{rev}) of the LIC (E_{rev} = +12 mV for TRP and –4 mV for TRPL). By contrast, Na^+/Ca^{2+} exchange currents should show exponential inward rectification (39) and would not be expected to reverse in response to an imposed Ca^{2+} load (11,40). To measure the current voltage (*I-V*) relationship of the tail currents, we applied voltage steps at the onset of tail current and subtracted a template recorded in the dark (Fig. 2). For comparison, the *I-V* relationship of the LIC was also measured in response to continuous dim red light illumination. Consistent with the properties of an exchanger, the tail current was inwardly rectifying (Fig. 2 *E*) and clearly

TABLE 1 Permeability ratios and theoretical P_f values of channels

Channels	Permeability ratios				
	P_{Ca}/P_{Cs}	P_{Mg}/P_{Cs}	P_{Na}/P_{Cs}	[a] P_K/P_{Cs}	P_f (%)
TRP (in *trpl*)	57.0	15.8	1.27	1.27	45.2
TRPL (in *trp*)	4.3	1.4	0.84	0.84	17.0
TRP+TRPL (in WT)	27.6	5.7	1.16	1.16	41.6

Permeability ratios (P_X/P_{Cs}) derived from reversal potential data (14,26). TRP channels were measured in *trpl* mutants, and TRPL channels were measured in *trp* mutants. The final column gives the fractional Ca^{2+} current (P_f) predicted by the GHK current equation (Eq. 1) at –70 mV expressed as the percentage of total LIC. P_{Na}/P_K was assumed to be 1.0.

[a]Under the experimental conditions, intracellular K^+ was substituted with Cs^+; P_K was not directly measured due to the large voltage-sensitive K^+ currents in *Drosophila* photoreceptors. However, increasing or decreasing the permeability ratio of K^+ by 2-fold had a negligible effect on predicted P_f in otherwise physiological solutions.

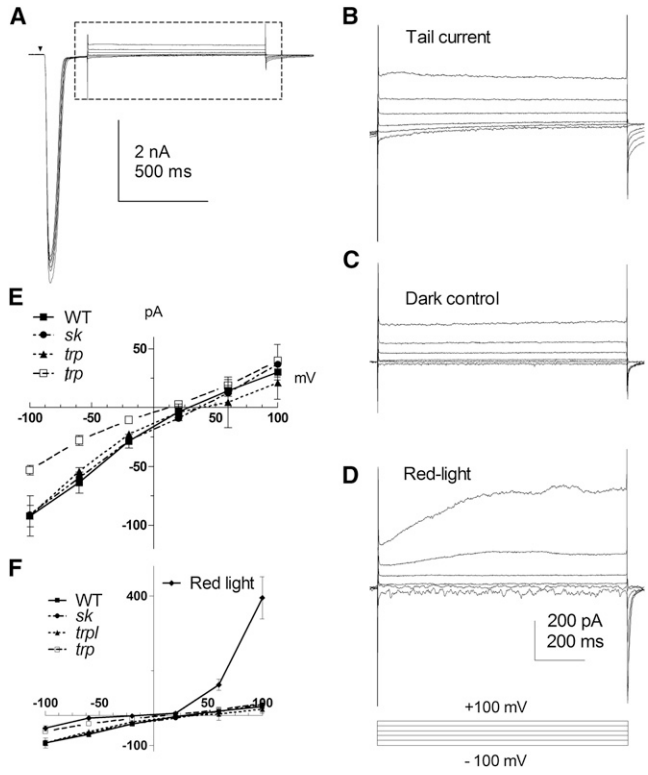

FIGURE 2 *I-V* relationships of tail currents. (*A*) Currents evoked by voltage steps from −100 mV to +100 mV (+40 mV steps) from a holding potential of −70 mV applied during tail currents of responses to flashes (5 ms, ~17,500 photons) in a *trpl* mutant. (*B*) Tail currents from the region indicated on an expanded scale. (*C*) Dark control currents to the same voltage steps. (*D*) Under continuous red light illumination, the strongly outwardly rectifying characteristics of the LIC are apparent. (*E*) *I-V* relationship of the tail currents obtained after subtracting dark control traces (as in *C*). The predominantly inward *I-V* curves of the tail currents are distinct from the strongly outwardly rectifying LIC shown in panel *F* (including the same tail current data on a different scale). No significant difference was seen among WT (n = 8), dSK^- (n = 5), and *trpl* (n = 2); smaller currents with otherwise similar properties were observed in *trp* (n = 5).

distinct from the strongly outwardly rectifying LIC (Fig. 2, *E* and *F*). Nevertheless, a small residual outward component was detected at depolarized voltages beyond +40 mV, possibly reflecting a residual, late inactivating light-induced component. However, this should not contribute significantly to the inward tail current at −70 mV, primarily because of the outward rectification and also because the kinetics of inactivation of the LIC are much faster at negative potentials due to the increased Ca^{2+} influx. Another potential contaminant of this current is the SK channel (small-conductance Ca^{2+}-activated K channel), which was recently reported in photoreceptors (32). However, a significant SK contribution can be effectively excluded because the *I-V* curve of the tail current in *sk* null mutants (*dSK*$^-$) was indistinguishable from that in the WT, whereas P_f values determined in *dSK*$^-$ flies were similar to those obtained in the WT (see Figs. 4 and 5).

The peak amplitude and charge integral of the inward tail current increased with flashes of increasing intensity (Fig. 3). The peak amplitudes (~100 pA) activated in WT and *trpl* were in line with previous measurements of the Na^+/Ca^{2+} exchange current (11). The peak amplitude of the tail current observed in *trp* was less than half of those (~40 pA), as would be expected if TRPL channels had a lower P_f. In all cases, the current decayed with a similar time course, which presumably represents the rate of Ca^{2+} extrusion via the exchanger (Fig. 3 *D*). In all cases, the time course was well fitted by a single- or double-exponential time course with a dominant time constant (τ_1) of ~300–400 ms and a minor slower component (τ_2 ~2 s).

Fractional Ca^{2+} current, P_f

Our method for measuring P_f assumes that all Ca^{2+} entering the cell through light-sensitive channels is extruded by the CalX exchanger. Having identified the slow inward tail current as a Na^+/Ca^{2+} exchange current, and assuming a stoichiometry of 3 Na^+:1 Ca^{2+}, which is generally accepted for NCX exchangers (27,41), we estimated P_f from the ratio between the total charge integral of the LIC and that of the CalX tail current (see Fig. 1 *B*).

Fig. 4 shows experimentally obtained values of P_f for TRP and/or TRPL channels from the WT and respective channel mutants compared with GHK predictions over a range of intensities. In principle, assuming the amount of

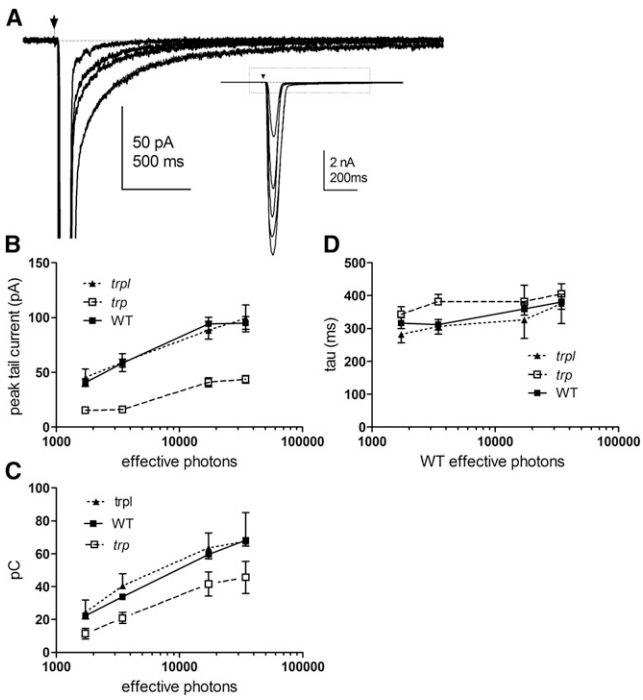

FIGURE 3 Intensity dependence of Na^+/Ca^{2+} exchange tail currents. (*A*) Responses recorded in WT photoreceptor to flashes (*arrow*) of increasing intensity (350, 1750, 3500, 17,500 and 35,000 effective photons). The inward tail component and main LIC (see *inset*) both increased with light intensity. (*B* and *C*) Mean peak amplitude (*B*) and charge integral (*C*) of the tail currents plotted as a function of intensity in WT, *trpl*, and *trp* mutants. (*D*) The single exponential decay time constant (τ) of the inward tail current was similar at all intensities and in different genetic backgrounds (WT, *trpl*, and *trp*). Mean values (mean ± SE) for WT (n = 20 cells), *trpl* (n = 6 cells), and *trp* (n = 8 cells).

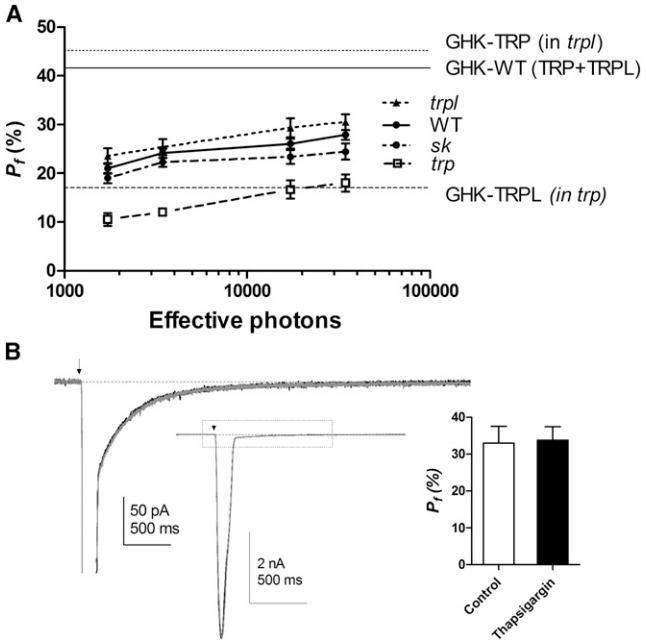

FIGURE 4 Measurement of fractional Ca^{2+} currents (P_f) through TRP and TRPL channels. (*A*) Mean P_f values (mean ± SE) are plotted as a function of intensity for TRP channels (isolated in *trpl*, n = 6), TRPL channels (isolated in *trp*, n = 8), native TRP+TRPL channels (in WT, n = 20), and TRP+TRPL channels (in *dSK*$^-$, n = 12). Empirical P_f data were obtained from the charge integral ratio between the total LIC and the exchanger tail current (see Materials and Methods), and compared with P_f predictions using the GHK equation (*horizontal lines*). (*B*) Responses to 5 ms flashes containing 17,500 photons (*arrow*) in the *trpl* photoreceptor were unaffected in the presence of 10 μM thapsigargin for >2–3 min (*gray* trace) compared with control exposed to vehicle (0.1% DMSO; *black* trace). The bar graph shows that P_f values in the presence of thapsigargin were indistinguishable from controls (n =3).

Ca^{2+} extruded by Na^{+}/Ca^{+} exchange equals the amount light-induced Ca^{2+} influx (42), P_f might be expected to remain constant with different intensities. However, we found that the empirical P_f values increased slightly with intensity. One factor that might contribute to this is that the exchanger is a low-affinity, high-capacity transporter that is expected to dominate Ca^{2+} homeostasis when Ca^{2+} levels are high: with lower Ca^{2+} levels associated with dimmer flashes, alternative higher-affinity transport and/or Ca^{2+} buffering mechanisms may prevent some Ca^{2+} ions from being immediately extruded by CalX exchange, leading to an underestimation of P_f. One such mechanism is sequestration of Ca^{2+} into smooth endoplasmic reticular (SER) stores by a SER Ca^{2+}-ATPase (43). To exclude this possibility, we measured P_f in *trpl* flies after applying the SERCA pump inhibitor thapsigargin (10 μM) by puffer pipette. No significant differences were found in the properties of either the light response or the CalX-dependent tail current (Fig. 4 *B*). Nevertheless, we cannot exclude minor contributions of nonelectrogenic Ca^{2+} mechanisms (e.g., plasma membrane Ca-ATPase), mitochondrial Ca^{2+} buffering, or high-affinity buffers that do not release Ca^{2+} on the timescale of the experiments (although we suggest that these may be less significant at higher intensities, where they are likely to be saturated by the higher Ca^{2+} concentrations).

The larger light-induced responses at higher intensities are increasingly subject to series resistance error and deteriorating space clamp, which may result in poor voltage-clamp control (see Discussion). As a compromise, therefore, we used P_f values derived from flashes of submaximal intensity (~17,500 photons, generating responses of <7 nA) from photoreceptors with optimal series compensation (>80%, $R_s < 25$ MΩ). On this basis, P_f for TRP channels, isolated in *trpl* mutants, was 29.3 ± 1.9% (mean ± SE, $n = 6$), which is substantial but still less than the simple GHK prediction of 45.2%. P_f for TRPL channels isolated in *trp* (16.6 ± 1.9% $n = 8$) was very close to the theoretical prediction (GHK-P_f = 17.0%). The WT current, which is mediated by both TRP and TRPL channels, yielded P_f values (26.1 ± 1.0%, $n = 20$) that were again below prediction (GHK-P_f = 41.6%). P_f in *dSk* null mutants (23.3 ± 1.5%, $n = 12$) was not significantly different from that in WT ($p > 0.05$). The results clearly confirm the higher fractional Ca^{2+} current mediated by TRP channels and support previous studies indicating that the WT LIC is largely carried by TRP under physiological conditions (14,31). Below, we consider the disparity between the empirical measurements and simple GHK predictions for TRP and WT currents by using a detailed modeling approach.

Voltage dependence of P_f

Thus far, P_f values were measured at resting potential (−70 mV); however, in vivo, photoreceptors depolarize in response to light. GHK theory predicts that P_f should vary with the membrane potential because each ion has its own unique reversal potential (E_{rev}). In addition, factors such as voltage-dependent divalent ion block (24) might influence P_f in a less predictable manner. We therefore measured P_f at different holding potentials. GHK theory predicts that P_f values should be almost constant at negative membrane potentials (−110 to −30 mV), but should tend to 100% near 0 mV as E_{rev} of monovalent ions is approached, while E_{rev} for Ca^{2+} remains positive. Unfortunately, we could not obtain accurate measurements at such positive potentials because the tail current was too small; however, within the range that could be tested, P_f was broadly independent of voltage in all genetic backgrounds, consistent with GHK theory (Fig. 5). This also implies that the high fractional Ca^{2+} current through the light-sensitive channels is maintained over most of the physiologically significant voltage operating range.

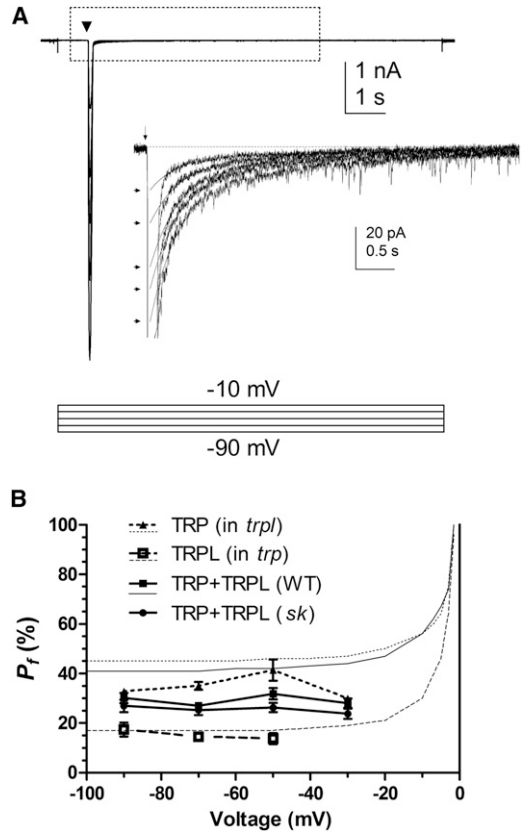

FIGURE 5 Voltage dependence of P_f. (*A*) Responses to bright 5 ms flashes (17,500 photons; *arrow*) in WT photoreceptor subjected to 10 s voltage steps (−90 mV to −10 mV in 20 mV steps) from a holding potential of −70 mV. Inset shows tail currents with exponential fits extrapolated back to time-to-peak of the LIC to estimate peak exchanger current (*arrows*). (*B*) P_f values (mean ± SE) as a function of membrane voltage in WT ($n = 10$), *trp* ($n = 5$), *trpl* ($n = 4$), and *dsK*$^{-}$ mutants ($n = 7$) compared with GHK-P_f (*continuous curves*). Consistent with theoretical predictions, empirical P_f values were broadly similar over the measured voltage range.

Ca^{2+} dependence of P_f

P_f is clearly predicted to increase with increasing extracellular Ca^{2+} concentration. To test this, we varied $[Ca^{2+}]_o$ without altering other cation concentrations by perfusing cells for 1–3 min using a puffer pipette before delivering test flashes. As previously reported, light responses in high $[Ca^{2+}]_o$ had faster time-to-peak and decay times (Fig. 6 *A*, *inset*) due to enhanced positive and negative feedback by Ca^{2+} (10). The peak amplitude of the exchanger current also significantly increased when $[Ca^{2+}]_o$ was raised, saturating above 3 mM at ~200 pA in WT and TRPL while continuing to increase up to at least 10 mM in *trp* mutants (Fig. 6 *B*). We also noted a change in the kinetics of the tail current, which no longer decayed exponentially at higher $[Ca^{2+}]_o$, but was initially ramp-like, probably indicating saturation of the exchanger rate (Fig. 6 *A*).

The simple GHK model predicts a sigmoidal increase in P_f for both TRP and TRPL channels approaching 100% at high $[Ca^{2+}]_o$. Our P_f measurements also increased in a Ca^{2+}-dependent fashion broadly in line with the GHK model (Fig. 6 *C*). As before, empirical P_f values closely approximated the GHK predictions for TRPL channels (in *trp*) across the tested $[Ca^{2+}]_o$ range, but were generally below them for TRP channel (in *trpl*) and the native TRP and TRPL channels (WT).

Modeling of Ca^{2+} dynamics

Although we confirmed the high fractional Ca^{2+} contribution to the LIC and the greater Ca^{2+} influx via TRP channels, we observed significant discrepancies between the empirical P_f values and simple GHK predictions, assuming static ionic concentrations. To explore the basis for this, we extended an earlier model of Ca^{2+} dynamics (9) that considers the diffusion, influx, and efflux of the ions involved in the light response (Ca^{2+}, Na^+, K^+, and Mg^{2+}) and takes into account the large local and global changes in extra- and intracellular ionic concentrations. Although the model is detailed, it only aims to reproduce the ionic fluxes in and out of a patch-clamped fly photoreceptor, under the conditions of our experiments, for a bright flash, which effectively produces a quantum bump in each microvillus in the rhabdomere (~35,000 effective photons). Using the model, we directly calculated estimates of fractional currents and tail currents caused by the Na^+/Ca^{2+} exchanger, taking into account dynamic changes in ionic concentration (see Supporting Material for details).

To model the concentration changes during the light response, we reduced the photoreceptor cell and extracellular space to a one-dimensional (1D) geometry consisting of a single microvillus connected to a representative section of the cell body, and an extramicrovillar space connected to a representative section of the intraommatidial cavity (Fig. 7). By further compartmentalizing this geometry, we were able to model diffusion, local ionic fluxes, and local Ca^{2+} buffering. We estimated the currents associated with the TRP and TRPL channels from three representative measurements for WT, *trp*, and *trpl* flies by subtracting an estimated exchanger current from the total LIC (Fig. S2). Based on these estimated channel currents, the modeled local ionic concentrations, the measured relative ionic permeabilities, and the GHK equation, we calculated the ionic fluxes through TRP and TRPL channels in and out of the microvillus (Figs. S3 and S4). We subsequently modeled

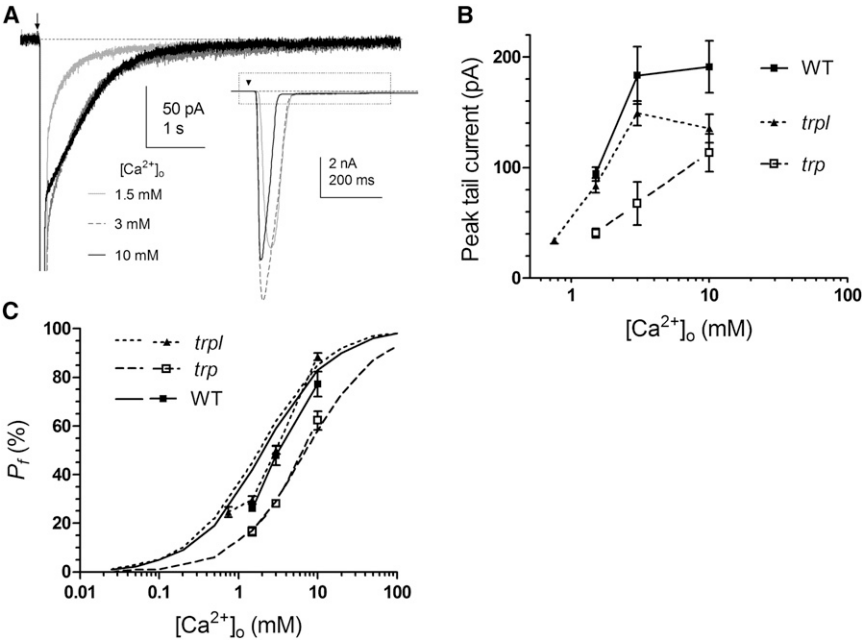

FIGURE 6 Ca^{2+} dependence of P_f. (*A*) Responses to 5 ms flashes (17,500 photons; *arrow*) recorded in different bath Ca^{2+} concentrations in *trpl* photoreceptors. Response kinetics became faster as Ca^{2+} was increased and resulted in a reduction of peak amplitude in most recordings. In addition to increasing in amplitude and area, the inward tail current was no longer well fit by an exponential at higher Ca^{2+} concentrations, but had an initial ramp-like phase indicative of saturation of the CalX exchanger. (*B*) Peak tail currents (mean ± SE) plotted as a function of $[Ca^{2+}]_o$ in WT, *trp*, and *trpl* mutants. (*C*) P_f values (*symbols*) at different Ca^{2+} concentrations compared with GHK-P_f predictions (*continuous curves*). Empirical P_f measurements increased in a Ca^{2+}-dependent manner broadly as predicted by GHK theory, but values for *trpl* and WT deviated from the quantitative predictions.

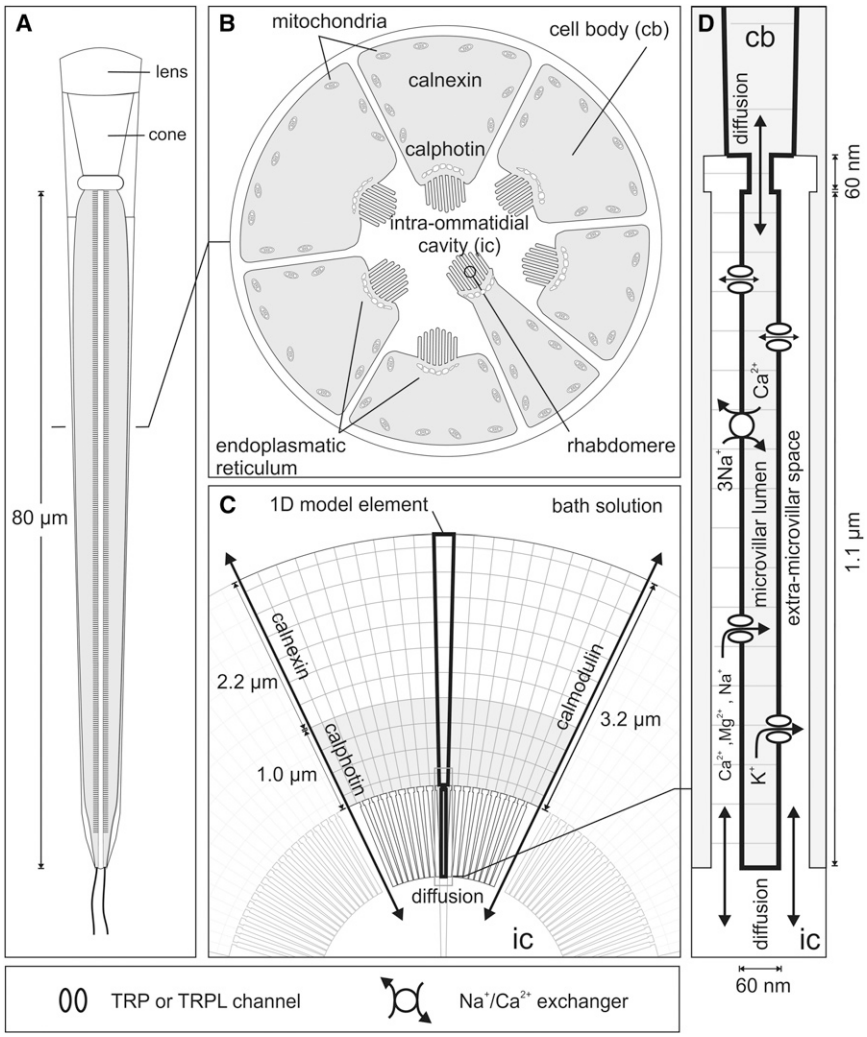

FIGURE 7 Photoreceptor geometry used for modeling. (*A* and *B*) Schematic of ommatidium in longitudinal view (A) and cross-section (*B*). (*C*) To model fluxes and diffusion, the geometry was reduced to a representative 1D element representing one microvillus and the associated section of cell body and extracellular space. (*D*) Schematic of microvillus with TRP/TRPL ion channels and Na^+/Ca^{2+} exchanger. For further details and dimensions, see Fig. S1 and Table S1.

intra- and extracellular diffusion of ions, the extrusion of Ca^{2+} ions by the Na^+/Ca^{2+} exchanger (Fig. S3A), and buffering of Ca^{2+} ions (Figs. S9 and S10). Because we used ouabain in all experiments, the model ignored any re-equilibration of Na^+ due to Na/K ATPase activity. We also ignored the dynamic reequilibration of Mg^{2+}, about which nothing is known in terms of photoreceptors. The absence of any tail current in *calx* mutants (Fig. 3) indicates at least that there is no significant electrogenic component.

The ionic fluxes, diffusion, and buffering led to concentration changes in the four compartments (Figs. S5–S8). When the TRP and TRPL channels opened, Ca^{2+}, Mg^{2+}, and Na^+ flowed into the cell, leading to a significant increase in the microvillus lumen and a delayed increase in the cell body after diffusion from the microvillus. Because Ca^{2+} ions are strongly buffered and have a lower diffusion coefficient than the other ions, Ca^{2+} showed a stronger peak in the microvillus, especially in WT and *trpl* flies, where influx was particularly high. Conversely, the concentration of Ca^{2+} ions decreased in the extracellular space, most notably in the extramicrovillar space and more moderately in the intraommatidial cavity. K^+ concentrations changed in the opposite direction, but by smaller amounts because K^+ has a high diffusion coefficient and its contribution to the LIC is small at -70 mV.

The Ca^{2+} concentration that is reached in the cell body depends strongly on the buffering power; therefore, we tuned the buffering power so that cell-body Ca^{2+} levels would peak around 50 μM in WT flies, as was previously measured using Ca^{2+} indicators (7). After Ca^{2+} influx, the exchanger extrudes the ions from the microvillus lumen into the extramicrovillar space in a concentration-dependent manner. The exchanger is assumed to saturate at high intracellular Ca^{2+} concentrations, with the concentration of half-maximal exchanger current tuned to a value of $K_X = 30$ μM. The maximal exchanger rate constant was adjusted to a value that is in agreement with the observed maximal exchanger current of ~200 pA. Apart from these exchanger parameters, the apparent rate of extrusion is predicted to depend strongly on Ca^{2+} diffusion from the cell body to

the microvillus/rhabdomere, which in turn is strongly influenced by the buffering power. Significantly, the same buffering parameters, which were tuned to reproduce the peak Ca^{2+} concentration in the cell body, also successfully modeled the time courses of the measured exchanger tail current, as well as Ca^{2+} concentration time courses previously measured using Ca^{2+} indicators (44,45).

The measured tail current exhibited a dominant fast component (τ ~300–400 ms) and a minor slow component (τ ~2 s). We explored several mechanisms to explain the second slow component, including diffusion from the pipette, mitochondria, and inhibition of the exchanger by intracellular Ca^{2+}. None of these mechanisms seemed to robustly reproduce the slow component in a way that was consistent with other aspects of the measurements. However, adding a low-capacity, moderately high-affinity Ca^{2+} buffer also gave a slow component and seemed to be in better agreement with other aspects of the measurements.

Tuning of parameters was based on a representative WT measurement obtained in a bath solution containing 1.5 mM Ca^{2+}. We subsequently used the same parameter set for the other simulations, in which we only varied the LIC (which was an input for the simulation); the relative permeabilities corresponding to WT, *trp*, and *trpl* flies; and the extracellular Ca^{2+} concentration. Because the measured integral of the LIC varies with extracellular Ca^{2+}, we scaled the representative LICs for WT, *trp*, and *trpl* flies measured in a bath solution containing 1.5 mM Ca^{2+}, with values of 0.6, 0.9, and 0.65 for simulations in which the Ca^{2+} bath concentration was 0.75, 3, and 10 mM, respectively.

Using the dynamic model, we calculated P_f values for WT, *trp*, and *trpl* flies for different extracellular Ca^{2+} concentrations and compared them with the measured values (Fig. 8 *A*). In similarity to the measured P_f values, we found that modeled P_f values in *trp* flies were hardly affected by dynamic changes in ion concentrations; however, for WT and *trpl* responses, we found that P_f was reduced close to measured values. During the peak of LIC, we predicted shifts in extra- and intracellular ionic concentrations (Figs. S6 and S7), which reduce the ionic gradients across the membrane and hence the driving force for ionic currents. The shifts were most notable in the confined extramicrovillar space and microvillus lumen. Although the gradients for Ca^{2+}, Mg^{2+}, and Na^{+} all became smaller, the effect on the more slowly diffusing Ca^{2+} combined with its large flux in WT and *trpl* flies was much more pronounced than that observed for Na^{+} and Mg^{2+}, and this reduced P_f by increasing the relative contribution of Na^{+} and to some extent Mg^{2+} compared with Ca^{2+} (Fig. S4).

Using the same dynamic model, we also calculated the exchanger tail currents for WT, *trp*, and *trpl* flies for the

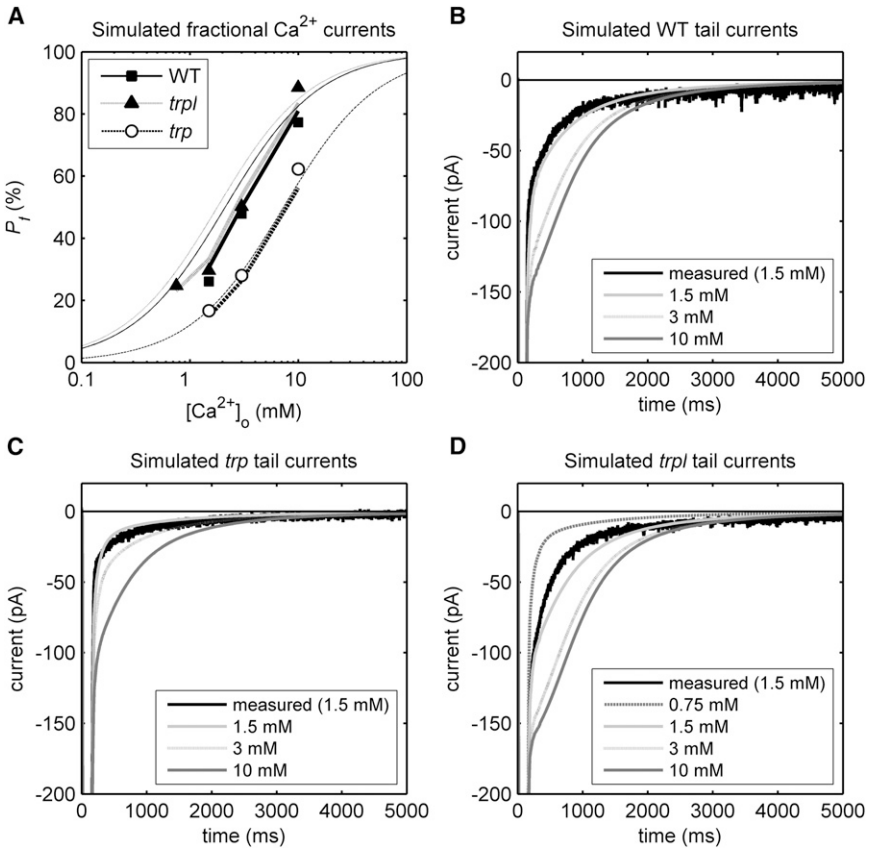

FIGURE 8 Dynamic modeling of fractional Ca^{2+} currents (P_f) and exchanger tail currents. (*A*) Comparison of simulated P_f values using the simple GHK model with static ionic concentrations (*thin continuous curves* replotted from Fig. 6), measured P_f values (*data point symbols*, replotted from Fig. 6) and the dynamic GHK model (*thick lines*, which fit well to the data points) for different extracellular Ca^{2+} concentrations in WT, *trpl*, and *trp*. With the dynamic GHK model, extracellular depletion of Ca^{2+} reduces the P_f calculated for WT and *trpl* flies compared with the simple GHK model. P_f values for *trp* flies are similar for both the simple and dynamic GHK models. (*B–D*) Measured tail currents for WT, *trpl*, and *trp* flies (*black*) with $[Ca^{2+}]_o$ = 1.5 mM, and modeled tail currents (*gray*) using the dynamic GHK model for different extracellular Ca^{2+} concentrations. The time course and amplitude of the tail currents are qualitatively consistent with measured tail currents. Notably, at higher extracellular Ca^{2+} concentrations, the tail currents for WT and *trpl* exhibit a ramp-like phase due to saturation of the exchanger, as also seen in measured tail currents (cf. Fig. 6).

different extracellular Ca^{2+} concentrations (Fig. 8, *B–D*). The peak exchanger current just after LIC was comparable to measured values. We also found that the time course of the measured tail current qualitatively agreed with the modeled tail current for all genetic backgrounds and Ca^{2+} concentrations, including the ramp-like decay at high extracellular Ca^{2+} concentrations indicative of exchanger saturation (Figs. 6 *A* and 8, *B* and *D*).

DISCUSSION

In this study, we characterize a light-induced tail current in *Drosophila* photoreceptors. We show that it is mediated by the CalX electrogenic Na^+/Ca^{2+} exchanger and exploit its properties to provide quantitative estimates of the fractional contribution of Ca^{2+} to the LIC (P_f) through TRP and TRPL channels. Our data confirm that Ca^{2+} influx represents a major component (~30%) of the LIC and is predominantly mediated by TRP channels, whereas TRPL channels mediate a more modest Ca^{2+} influx. The voltage and Ca^{2+} dependence of P_f are broadly in line with predictions of GHK theory, and the P_f for the TRPL channel closely matches that predicted by GHK theory. However, although the P_f of TRP channels (~30%) was ~2 times greater than that of TRPL, it was substantially lower than the simple GHK prediction (45%). A detailed model incorporating intra- and extracellular geometry, ion permeation, diffusion, extrusion, and buffering suggested that this deviation from the GHK prediction could be largely accounted for by extracellular ionic depletion during the large LICs.

Methodological considerations

The standard approach for measuring P_f involves loading cells with saturating levels of Ca^{2+} indicator dyes, which then must be calibrated, ideally using a pure Ca^{2+} current (22). This approach is impractical for *Drosophila* photoreceptors because of the huge Ca^{2+} fluxes, the extreme compartmentalization, and the lack of a pure Ca^{2+} current control for calibration. We therefore developed an alternative method based on the endogenous Na^+/Ca^{2+} exchanger. This method assumes that all Ca^{2+} entering the cell is removed by the CalX exchanger during the time course of the tail current. In a strict sense, this is unlikely to be completely true (see below); however, there is a substantial body of evidence implicating the CalX exchanger as the principal mechanism of Ca^{2+} extrusion in *Drosophila* photoreceptors (29,42). The rapidity and high efficiency of Na^+/Ca^{2+} exchange has also been demonstrated in *Drosophila* photoreceptors by a near-instantaneous inward exchange current that can be evoked by photolytic release of caged Ca^{2+} (11).

The method also assumes that the light-induced rise in Ca^{2+} is entirely due to Ca^{2+} influx through TRP and/or TRPL channels, and that other modes of raising cytosolic Ca^{2+} levels are negligible. This is strongly supported by studies using Ca^{2+} indicator dyes, in which it was concluded that Ca^{2+} influx vastly outweighs any release from intracellular stores (5–7,46). We also found that our estimate of P_f was unaffected by first depleting intracellular stores with thapsigargin. This result also excludes significant long-term Ca^{2+} sequestration by the SERCA pump as a source of error in our measurements.

Intensity dependence of P_f

In our experiments, we observed a slight intensity-dependent rise in P_f values (Fig. 4) that was not necessarily predicted, although a similar intensity-dependent difference between light-induced Ca^{2+} influx and Na^+/Ca^{2+} exchange-dependent efflux has also been reported in blowfly photoreceptors (37). One possible explanation for the variation of P_f with intensity is a significant contribution of alternative, higher-affinity Ca^{2+} homeostatic mechanisms (e.g., buffers, stores, mitochondria, transporters) at lower intensities. It is possible that certain Ca^{2+}-buffering/sequestering components have a slower release time constant and that some Ca^{2+} is not rapidly extruded by Na^+/Ca^+ exchange, but rather is released on a slower timescale and/or extruded by nonelectrogenic transporters such as the high-affinity plasma membrane Ca-ATPase. A significant contribution from any of these components would lead to an underestimation of P_f. With higher-intensity flashes, the empirical P_f estimate may approach its true value due to a greater proportion of high-affinity sites being occupied or saturated, leading to increased reliance on the low-affinity, high-capacity exchanger.

Another possibility is that the large currents elicited by brighter flashes were inadequately voltage-clamped, owing to series resistance (R_s) errors (maximally 40–50 mV) and/or poor space-clamp conditions. Both GHK theory and direct measurements suggest that the effect of voltage on P_f is minimal at hyperpolarized potentials below −20 mV (Fig. 5); however, P_f is predicted to increase sharply above −20 mV, and we cannot entirely exclude the possibility that voltage-clamp control of some of the largest responses may have deteriorated sufficiently to increase the P_f.

Finally, although the total LIC is smaller at low intensities, the local current density (number of channels activated per photon per microvillus) actually increases. Hence, in principle, local ionic depletion could be higher at low intensities, leading to greater deviation from the GHK prediction (i.e., the P_f value decreases at low intensity). However, this effect would be offset by less global depletion of the overall extracellular space, and the situation cannot be directly modeled by our assumption of a repeating 1D element (which strictly holds only for the case in which each microvillus is activated once).

Modeling Ca^{2+} influx and extrusion

Our experimentally obtained P_f values closely matched simple GHK predictions for TRPL channels but not for TRP channels. Although this might indicate that the GHK assumptions had been violated for TRP, a detailed model suggested that the discrepancy could be largely explained by extracellular ion depletion. Thus, a computational model that still uses GHK theory but calculates dynamic ionic concentrations by taking into account photoreceptor cell geometry was able to robustly reproduce the observed P_f values and Na^+/Ca^{2+} exchanger tail currents over a range of extracellular Ca^{2+} concentrations and different genetic backgrounds. Because Ca^{2+} is a major charge carrier in WT and *trpl* flies, and also has the lowest diffusion coefficient, it is more strongly depleted in the extracellular space during the peak response than Na^+ and Mg^{2+}, resulting in a lower P_f in WT and *trpl* flies. In *trp* flies, the contribution of Ca^{2+} to the total current is lower and hence Ca^{2+} is less depleted, resulting in only a slightly smaller P_f value.

An essential feature of our model is the inclusion of Ca^{2+} buffering in the cell body. To obtain a realistic peak Ca^{2+} (50 μM) in the cell body, Ca^{2+} must be strongly (90–98%) buffered (without buffering, Ca^{2+} is expected to reach ~0.5 mM in the cell body). Apart from controlling cell-body concentrations, buffering also slows down extrusion of Ca^{2+} and diffusion from the cell body to the rhabdomere. The time constant for free diffusion from the cell body to the rhabdomere is estimated to be approximately $\tau = 4/\pi^2 \times d_{cb}^2/D_{Ca^{2+}} = 4/\pi^2 \times 3.2^2/220 = 19$ ms, but for buffered Ca^{2+} this can be ~200–400 ms and even slower, suggesting that extrusion is partly diffusion limited. Significantly, the latter time constant matches the dominant time constant observed in the Na^+/Ca^{2+} exchanger tail current. In other words, the introduction of a Ca^{2+} buffer with properties needed to account for measured cell-body Ca^{2+} concentrations also yields the observed extrusion time constant without further tuning. This interpretation of the effect of buffering on time constants is also consistent with a recent study that reported a similar time constant (~350 ms) for the increase in cell-body Ca^{2+} after illumination, which was accelerated to ~20 ms after genetic knockdown of the major cell-body Ca^{2+}-binding protein calphotin (45).

To account for the maximal exchanger current of ~200 pA, we modeled the exchanger using a Hill coefficient of one and a concentration of half-maximal exchanger current of $K_X = 30$ μM. Qualitatively, this yielded the correct time course and shape of the exchanger tail current for all extracellular Ca^{2+} concentrations and genetic backgrounds, including similar saturation characteristics (ramp-like decay) just after the peak currents recorded in high $[Ca^{2+}]_o$ (3 and 10 mM; cf. Figs. 6 and 8). The value for K_X is higher than the values reported for regulatory and transport binding sites for other organisms (41). However, it is likely that the apparent IC_{50} values are different from specific binding sites, and, moreover, other ions or regulatory mechanisms may also affect the apparent affinity in vivo. From a physiological viewpoint, a relatively low apparent affinity of the exchanger for intracellular Ca^{2+} would be beneficial for cells that have to handle large Ca^{2+} influxes leading to concentration changes in the order of tens of micromolars. In some organisms at least, NCX exchangers can be modulated by $[Na^+]_o$, $[Na^+]_i$, or $[Ca^{2+}]_o$ (41,47). For simplicity, we ignored such regulatory sites because *Drosophila* CalX has not been fully characterized in this respect, and because these concentrations only undergo only relatively small changes during the light response compared with the massive changes in $[Ca]_i$.

CONCLUSIONS

To our knowledge, our results represent the first empirical measurements of the fractional Ca^{2+} current (P_f) of the light-sensitive channels in *Drosophila*. Because the TRP channel in particular shows complex permeation properties and divalent ion block, it is unlikely to strictly obey the assumptions (e.g., independent mobility of ions) of GHK theory. Despite this, our results indicate that to a good approximation, the fractional Ca^{2+} current follows the GHK prediction for both TRP and TRPL. It is only reduced from the simple GHK prediction for the case of TRP channels because of the depletion of Ca^{2+} ions that occurs during responses to bright flashes. Despite this reduction in P_f, Ca^{2+} influx is still massive. For example, assuming a single-channel conductance of 8 pS (48), a P_f of 30% represents a flux of ~600 Ca^{2+} ions/ms per TRP channel at resting potential. Within the volume of a microvillus (~3×10^{-18} liter), this represents an unbuffered flux of 350 μM/ms per channel. During the peak responses to the bright flashes used in this study, our model predicts that microvillar Ca^{2+} will transiently reach ~0.5 mM in WT and *trpl* photoreceptors, and ~0.15 mM in *trp* (Fig. S6). In response to these bright flashes, each effectively absorbed photon generates an average response of <1 pA. This is much smaller than the normal single-photon response (quantum bump), because the global rise in Ca^{2+} initiated by bumps with the shortest latencies already attenuates (light adapts) the majority of bumps that arise with longer latencies. Under dim illumination, single quantum bumps have an amplitude of ~10 pA representing the opening of ~15 channels in a single microvillus, and we predict that free Ca^{2+} transiently reaches levels of several millimolars within individual microvilli, as previously proposed (9). Under light-adapted conditions, each effectively absorbed photon may now only activate a single channel for a few milliseconds, but even this would be expected to raise microvillar free Ca^{2+} transiently well above 10 μM.

Although the model was specifically implemented to provide insight into the Ca^{2+} fluxes and exchanger currents associated with our bright-flash experiments, successful

modeling of the exchanger tail current also provided insight into the cytosolic Ca^{2+} buffering of the cell body and microvilli. Particularly important are immobile cytosolic buffers, the most significant of which is probably the Ca^{2+}-binding protein calphotin, which is localized in a band at the base of the microvilli (45,49,50). To account for both the measured exchanger time constant and the control of absolute cytosolic Ca^{2+} in the face of massive Ca^{2+} influx, the modeling suggests that the buffer (putatively calphotin) should have a relatively low affinity (~1 mM) and high local concentration (20 mM). Future implementation of the model should provide the framework for gaining a more detailed understanding of Ca^{2+} homeostasis in microvillar photoreceptors under more physiological conditions, i.e., by considering reequilibration of Na^{+} via Na/K ATPase in the voltage domain rather than under voltage clamp, and responses to more physiologically relevant illumination.

SUPPORTING MATERIAL

Supporting analysis, figures, tables, and references (51-62) are available at http://www.biophysj.org/biophysj/supplemental/S0006-3495(13)00386-X.

This research was supported by the Biotechnology and Biological Sciences Research Council (grant BB/G006865/1 to R.C.H. and a doctoral award to B.C.) and the Netherlands Research Organization (NWO-ALW VIDI 864.09.015 to M.P.).

REFERENCES

1. Katz, B., and B. Minke. 2009. *Drosophila* photoreceptors and signaling mechanisms. *Front Cell Neurosci.* 3:2.
2. Wang, T., and C. Montell. 2007. Phototransduction and retinal degeneration in *Drosophila*. *Pflugers Arch.* 454:821–847.
3. Yau, K. W., and R. C. Hardie. 2009. Phototransduction motifs and variations. *Cell.* 139:246–264.
4. Hardie, R. C., and M. Postma. 2008. Phototransduction in microvillar photoreceptors of Drosophila and other invertebrates. *In* The Senses—A Comprehensive Reference. Vision I, Vol. 1. T. D. Albright and R. Masland, editors. Academic Press, Oxford. 77–130.
5. Ranganathan, R., B. J. Bacskai, …, C. S. Zuker. 1994. Cytosolic calcium transients: spatial localization and role in *Drosophila* photoreceptor cell function. *Neuron.* 13:837–848.
6. Peretz, A., E. Suss-Toby, …, B. Minke. 1994. The light response of *Drosophila* photoreceptors is accompanied by an increase in cellular calcium: effects of specific mutations. *Neuron.* 12:1257–1267.
7. Hardie, R. C. 1996. INDO-1 measurements of absolute resting and light-induced Ca^{2+} concentration in *Drosophila* photoreceptors. *J. Neurosci.* 16:2924–2933.
8. Oberwinkler, J., and D. G. Stavenga. 2000. Calcium transients in the rhabdomeres of dark- and light-adapted fly photoreceptor cells. *J. Neurosci.* 20:1701–1709.
9. Postma, M., J. Oberwinkler, and D. G. Stavenga. 1999. Does Ca^{2+} reach millimolar concentrations after single photon absorption in *Drosophila* photoreceptor microvilli? *Biophys. J.* 77:1811–1823.
10. Hardie, R. C. 1991. Whole-cell recordings of the light-induced current in *Drosophila* photoreceptors: evidence for feedback by calcium permeating the light sensitive channels. *Proc. Biol. Sci.* 245:203–210.
11. Hardie, R. C. 1995. Photolysis of caged Ca^{2+} facilitates and inactivates but does not directly excite light-sensitive channels in *Drosophila* photoreceptors. *J. Neurosci.* 15:889–902.
12. Gu, Y., J. Oberwinkler, …, R. C. Hardie. 2005. Mechanisms of light adaptation in *Drosophila* photoreceptors. *Curr. Biol.* 15:1228–1234.
13. Hardie, R. C., and B. Minke. 1992. The *trp* gene is essential for a light-activated Ca^{2+} channel in *Drosophila* photoreceptors. *Neuron.* 8:643–651.
14. Reuss, H., M. H. Mojet, …, R. C. Hardie. 1997. In vivo analysis of the *drosophila* light-sensitive channels, TRP and TRPL. *Neuron.* 19:1249–1259.
15. Hardie, R. C., P. Raghu, …, S. T. Sweeney. 2001. Calcium influx via TRP channels is required to maintain PIP_2 levels in *Drosophila* photoreceptors. *Neuron.* 30:149–159.
16. Liu, C. H., A. K. Satoh, …, R. C. Hardie. 2008. Ca^{2+}-dependent metarhodopsin inactivation mediated by calmodulin and NINAC myosin III. *Neuron.* 59:778–789.
17. Wu, C. F., and W. L. Pak. 1978. Light-induced voltage noise in the photoreceptor of *Drosophila melanogaster*. *J. Gen. Physiol.* 71:249–268.
18. Juusola, M., and R. C. Hardie. 2001. Light adaptation in *Drosophila* photoreceptors: I. Response dynamics and signaling efficiency at 25°C. *J. Gen. Physiol.* 117:3–25.
19. Pumir, A., J. Graves, R. Ranganathan, and B. I. Shraiman. 2008. Systems analysis of the single photon response in invertebrate photoreceptors. *Proc. Natl. Acad. Sci. USA.* 105:10354–10359.
20. Nikolic, K., J. Loizu, …, C. Toumazou. 2010. A stochastic model of the single photon response in *Drosophila* photoreceptors. *Integr Biol (Camb).* 2:354–370.
21. Song, Z., M. Postma, …, M. Juusola. 2012. Stochastic, adaptive sampling of information by microvilli in fly photoreceptors. *Curr. Biol.* 22:1371–1380.
22. Schneggenburger, R., Z. Zhou, …, E. Neher. 1993. Fractional contribution of calcium to the cation current through glutamate receptor channels. *Neuron.* 11:133–143.
23. Hille, B. 2001. Ionic Channels in Excitable Membranes. Sinauer, Sunderland, MA.
24. Hardie, R. C., and M. H. Mojet. 1995. Magnesium-dependent block of the light-activated and *trp*-dependent conductance in *Drosophila* photoreceptors. *J. Neurophysiol.* 74:2590–2599.
25. Parnas, M., B. Katz, and B. Minke. 2007. Open channel block by Ca^{2+} underlies the voltage dependence of *drosophila* TRPL channel. *J. Gen. Physiol.* 129:17–28.
26. Liu, C. H., T. Wang, …, R. C. Hardie. 2007. In vivo identification and manipulation of the Ca^{2+} selectivity filter in the *Drosophila* transient receptor potential channel. *J. Neurosci.* 27:604–615.
27. Hinata, M., H. Yamamura, …, J. Kimura. 2002. Stoichiometry of Na^{+}-Ca^{2+} exchange is 3:1 in guinea-pig ventricular myocytes. *J. Physiol.* 545:453–461.
28. Hryshko, L. V., S. Matsuoka, …, K. D. Philipson. 1996. Anomalous regulation of the *Drosophila* $Na(^{+})$-Ca^{2+} exchanger by Ca^{2+}. *J. Gen. Physiol.* 108:67–74.
29. Wang, T., H. Xu, …, C. Montell. 2005. Light activation, adaptation, and cell survival functions of the Na^{+}/Ca^{2+} exchanger CalX. *Neuron.* 45:367–378.
30. Scott, K., Y. M. Sun, …, C. S. Zuker. 1997. Calmodulin regulation of *Drosophila* light-activated channels and receptor function mediates termination of the light response in vivo. *Cell.* 91:375–383.
31. Niemeyer, B. A., E. Suzuki, …, C. S. Zuker. 1996. The *Drosophila* light-activated conductance is composed of the two channels TRP and TRPL. *Cell.* 85:651–659.
32. Abou Tayoun, A. N., X. Li, …, P. J. Dolph. 2011. The Drosophila SK channel (dSK) contributes to photoreceptor performance by mediating sensitivity control at the first visual network. *J. Neurosci.* 31:13897–13910.

33. Hardie, R. C., F. Martin, …, P. Raghu. 2002. Molecular basis of amplification in Drosophila phototransduction: roles for G protein, phospholipase C, and diacylglycerol kinase. *Neuron.* 36:689–701.

34. Ruknudin, A., C. Valdivia, …, D. H. Schulze. 1997. Na^{+}/Ca^{2+} exchanger in *Drosophila*: cloning, expression, and transport differences. *Am. J. Physiol.* 273:C257–C265.

35. Schwarz, E. M., and S. Benzer. 1997. Calx, a Na-Ca exchanger gene of *Drosophila melanogaster*. *Proc. Natl. Acad. Sci. USA*. 94:10249–10254.

36. Minke, B., and E. Armon. 1984. Activation of electrogenic Na-Ca exchange by light in fly photoreceptors. *Vision Res.* 24:109–115.

37. Gerster, U. 1997. A quantitative estimate of flash-induced $Ca(^{2+})$- and $Na(^{+})$-influx and $Na^{+}/Ca(^{2+})$-exchange in blowfly *Calliphora* photoreceptors. *Vision Res.* 37:2477–2485.

38. Jansonius, N. M. 1990. Properties of the sodium-pump in the blowfly photoreceptor cell. *J. Comp. Physiol. A Neuroethol. Sens. Neural Behav. Physiol.* 167:461–467.

39. Lipp, P., and L. Pott. 1988. Voltage dependence of sodium-calcium exchange current in guinea-pig atrial myocytes determined by means of an inhibitor. *J. Physiol.* 403:355–366.

40. Niggli, E., and W. J. Lederer. 1993. Activation of Na-Ca exchange current by photolysis of "caged calcium". *Biophys. J.* 65:882–891.

41. Blaustein, M. P., and W. J. Lederer. 1999. Sodium/calcium exchange: its physiological implications. *Physiol. Rev.* 79:763–854.

42. Oberwinkler, J., and D. G. Stavenga. 2000. Calcium imaging demonstrates colocalization of calcium influx and extrusion in fly photoreceptors. *Proc. Natl. Acad. Sci. USA*. 97:8578–8583.

43. Walz, B. 1982. Calcium-sequestering smooth endoplasmic reticulum in retinula cells of the blowfly. *J. Ultrastruct. Res.* 81:240–248.

44. Rosenbaum, E. E., R. C. Hardie, and N. J. Colley. 2006. Calnexin is essential for rhodopsin maturation, Ca^{2+} regulation, and photoreceptor cell survival. *Neuron.* 49:229–241.

45. Weiss, S., E. Kohn, …, B. Minke. 2012. Compartmentalization and Ca^{2+} buffering are essential for prevention of light-induced retinal degeneration. *J. Neurosci.* 32:14696–14708.

46. Cook, B., and B. Minke. 1999. TRP and calcium stores in *Drosophila* phototransduction. *Cell Calcium.* 25:161–171.

47. Weber, C. R., K. S. Ginsburg, …, D. M. Bers. 2001. Allosteric regulation of Na/Ca exchange current by cytosolic Ca in intact cardiac myocytes. *J. Gen. Physiol.* 117:119–131.

48. Henderson, S. R., H. Reuss, and R. C. Hardie. 2000. Single photon responses in *Drosophila* photoreceptors and their regulation by Ca^{2+}. *J. Physiol.* 524:179–194.

49. Ballinger, D. G., N. Xue, and K. D. Harshman. 1993. A *Drosophila* photoreceptor cell-specific protein, calphotin, binds calcium and contains a leucine zipper. *Proc. Natl. Acad. Sci. USA*. 90:1536–1540.

50. Martin, J. H., S. Benzer, …, C. A. Miller. 1993. Calphotin: a *Drosophila* photoreceptor cell calcium-binding protein. *Proc. Natl. Acad. Sci. USA*. 90:1531–1535.

51. Suzuki, E., E. Katayama, and K. Hirosawa. 1993. Structure of photoreceptive membranes of *Drosophila* compound eyes as studied by quick-freezing electron microscopy. *J. Electron Microsc. (Tokyo).* 42:178–184.

52. Kushmerick, M. J., and R. J. Podolsky. 1969. Ionic mobility in muscle cells. *Science.* 166:1297–1298.

53. Allbritton, N. L., T. Meyer, and L. Stryer. 1992. Range of messenger action of calcium ion and inositol 1,4,5-trisphosphate. *Science.* 258:1812–1815.

54. Li, Y., and S. Gregory. 1974. Diffusion of ions in sea water and in deep-sea sediments. *Geochim. Cosmochim. Acta.* 38:703–714.

55. Porter, J. A., M. Yu, …, C. Montell. 1993. Dependence of calmodulin localization in the retina on the NINAC unconventional myosin. *Science.* 262:1038–1042.

56. Maune, J. F., C. B. Klee, and K. Beckingham. 1992. Ca^{2+} binding and conformational change in two series of point mutations to the individual $Ca(^{2+})$-binding sites of calmodulin. *J. Biol. Chem.* 267:5286–5295.

57. Paulsen, R., D. Zinkler, and M. Delmelle. 1983. Architecture and dynamics of microvillar photoreceptor membranes of a cephalopod. *Exp. Eye Res.* 36:47–56.

58. Zinkler, D., J. Bentrop, and R. Paulsen. 1985. Phospholipids of fly photoreceptor membrane: fatty acid and phosphoinositide metabolism. *Verh. Dtsch. Zool. Ges.* 78:303.

59. McLaughlin, S., and J. E. Brown. 1981. Diffusion of calcium ions in retinal rods. A theoretical calculation. *J. Gen. Physiol.* 77:475–487.

60. Oberwinkler, J. 2002. Calcium homeostasis in fly photoreceptor cells. *Adv. Exp. Med. Biol.* 514:539–583.

61. Mojet, M. H., J. Tinbergen, and D. G. Stavenga. 1992. Receptor potential and light-induced mitochondrial activation in blowfly photoreceptor mutants. *J. Comp. Physiol. A Neuroethol. Sens. Neural Behav. Physiol.* 168:305–312.

62. Peretz, A., C. Sandler, …, B. Minke. 1994. Genetic dissection of light-induced Ca^{2+} influx into *Drosophila* photoreceptors. *J. Gen. Physiol.* 104:1057–1077.

Supporting Materials:

Fractional Ca^{2+} currents of TRP and TRPL channels through Drosophila photoreceptors

Brian Chu[1], Marten Postma[2] and Roger C Hardie[1]

[1]*Cambridge University Department of Physiology Development and Neuroscience, Downing St Cambridge CB23EG U.K.*

[2] *Molecular Cytology, Swammerdam Institute for Life Sciences, University of Amsterdam Science Park 904, NL-1098 XH Amsterdam The Netherlands*

MODELLING IONIC DYNAMICS IN THE FLY PHOTORECEPTOR CELL

This model aims to capture the ionic fluxes in and out of a patch-clamped fly photoreceptor cell after a strong light flash, which effectively produces a quantum bump in each microvillus in the rhabdomere. The model, which is an extension of previously published models (1-3), describes the diffusion, influx and efflux of the Ca^{2+}, Na^{+}, K^{+} and Mg^{2+} ions that are involved in the light response. Using the model we can directly calculate an estimate of the fractional currents and the tail current caused by the electrogenic Na^{+}/Ca^{2+} exchanger, explicitly taking into account any local and global changes in ionic concentrations

After light induced activation of TRP and TRPL channels there is a rapid influx and fast intracellular increase of Ca^{2+}, Mg^{2+} and Na^{+} ions in the rhabdomere and subsequently in the cell-body, and a decrease in K^{+} ions . Conversely, a significant decrease of Ca^{2+}, Mg^{2+} and Na^{+} and an increase of K^{+} concentrations is expected in the relatively confined extracellular space between the microvilli and in the intra-ommatidial cavity during the initial light response. During and after the activation of TRP and TRPL channels, the electrogenic Na^{+}/Ca^{2+} exchanger will extrude the excess Ca^{2+} ions from the photoreceptor cell in exchange for three times as many Na^{+} ions. The action of the exchanger can be directly observed as a tail current. The dynamics of Ca^{2+} ions differs from that of the other ions because they are much more strongly buffered by intracellular (and extracellular) calcium buffers, which will reduce the observed transient levels of free Ca^{2+} ion concentrations and will also slow down the kinetics of Ca^{2+} (fluxes and diffusion).

Below we describe the details of the model assumptions and used parameter values. Firstly, we describe the geometry used in the simulations, where we reduce the 3D geometry into an effective 1D geometry that captures the basic properties of the spatio-temporal process

of diffusion and ionic fluxes between the intracellular and extracellular space. Secondly, we describe all ionic fluxes that contribute. Thirdly, we describe the diffusion coefficients that were used. Fourthly, we describe the different components that contribute to the intracellular and extracellular buffering of Ca^{2+} ions. Finally, we describe the transport equations used in the model and how these were discretized and numerically integrated. The last section shows the results of simulations for WT, *trp* and *trpl* flies.

Detailed description of the geometry We divided the intracellular space into two compartments. The first compartment is the microvillus, which is represented by a slender cylinder with an average length L_m = 1.1 µm and an inner radius $r_{m,i}$ = 26 nm. The microvillus is connected to the cell body by a narrow cylindrical shaped neck, which has a length L_n = 60 nm and an inner radius $r_{n,i}$ = 14 nm. The cell body is represented by a section of a cylinder, which spans an angle α_{cb} = 360 º /N_{cell} = 51.4º, has an effective intra-ommatidial radius r_{ic} = 2.8 µm and an outer ommatidial radius r_{om} = 6 µm. The radial diameter of the cell body is then $d_{cb} = r_{om} - r_{ic}$ = 3.2 µm, and the diameter in the angular direction changes from 2.5 µm to 5.4 µm. The average volume of the cell-body is $V_{cb} = \left(\pi r_{om}^2 - \pi r_{ic}^2\right) L_{cell} / N_{cell}$ = 1.01 pl, where L_{cell} = 80 µm denotes the length of the photoreceptor cell and N_{cell} the number of photoreceptor cells in a single ommatidium (Fig. S1A,B). The rhabdomere, with radius r_{rh} = 0.75 µm, consists of a staggered array of about N_{micro} = 35,000 tightly packed touching microvilli, each row is separated by a distance Δy = 48 nm and comprises about $N_{micro,row}$ = 21 microvilli (Fig. S1B, C). Each column is separated by a distance Δx = 74 nm and comprises about $N_{micro,column}$ = 1667 microvilli. All microvilli are distributed equally over the cell-body volume in such a way that each microvillus is connected to a subsection of the cell-body, with height Δy = 48 nm and angle $\Delta\alpha_{cb} = \alpha_{cb} / N_{micro,row}$ = 2.45º.

The extracellular space also consists of two compartments (Fig. S1C,G). The first compartment is the space between the microvilli in the rhabdomere. The volume of this extra-microvillar space is estimated to be about 20% of the intracellular microvillus volume. The extra-microvillar space is connected directly to the intra-ommatidial cavity, which is surrounded by the seven photoreceptor cells in the ommatidium (in a cross section). The intra-ommatidial cavity has a complex geometry; because we assume diffusion is fast in the intra-ommatidial cavity we modelled this as a cylinder with an effective radius r_{ic} = 2.8 µm. The volume of the intra-ommatidial cavity is $V_{ic} = \left(\pi r_{ic}^2 - N_{cell}\pi r_{rh}^2\right) L_{cell}$ = 0.91 pl.

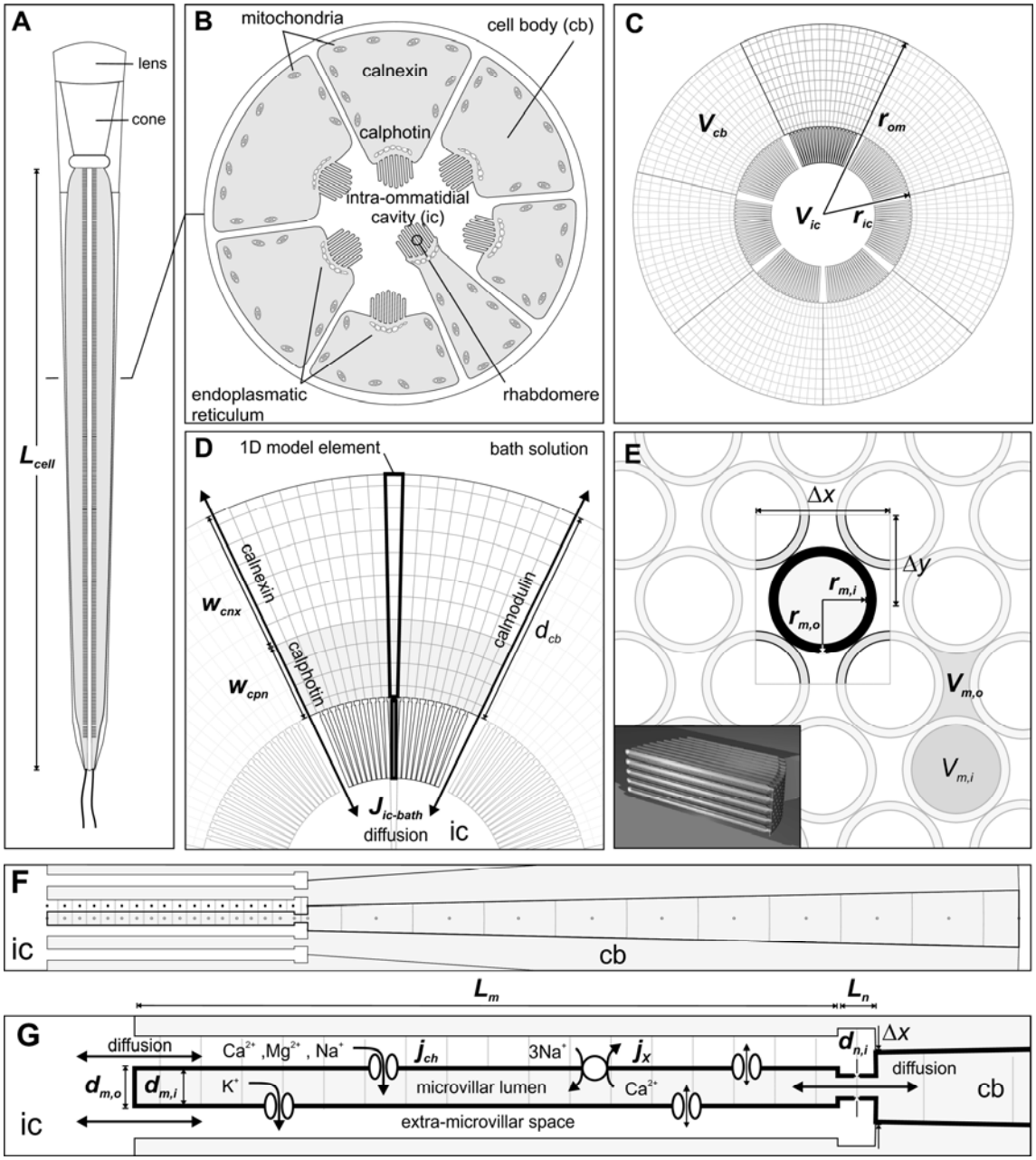

FIGURE S1: Geometry of ommatidium and photoreceptor (*A*) Schematic of ommatidium (*B*) Schematic cross-section of ommatidium (*C*) Idealized geometry of ommatidium and (*D*) one photoreceptor composed of multiple repeats of a single 1D model element. (*E*) packing geometry of microvilli in cross-section; inset: schematic showing 3D stacking of microvilli. (*F*) Single compartmentalized 1D element used for modelling (*G*) Detail of microvillus showing channels and NCX exchanger. See Table S1 for values and definitions of various symbols and dimensions. The symbols $d_{m,o}$, $d_{m,i}$ and $d_{n,i}$ in panel G represent diameters, which are twice the corresponding radii defined in table S1.

TABLE I: Geometrical parameters used in the simulations

parameter	value	Unit	Description	reference
$r_{m,i}$	26	nm	Inner radius of microvillus	(4)
$r_{m,o}$	30	nm	Outer radius of microvillus	(4)
L_m	1.1	µm	Average microvillus length	
$r_{n,i}$	14	nm	Inner radius of microvillus neck	(4)
L_n	60	nm	Approximate neck length	(4)
N_{cell}	7	-	Number of photoreceptor cells per ommatidium	
r_{om}	6	µm	Effective radius of ommatidium	
r_{ic}	2.8	µm	Effective radius of intra-ommatidial cavity	
d_{cb}	3.2	µm	Radial diameter of cell-body	$d_{cb} = r_{om} - r_{ic}$
r_{rh}	0.75	µm	Radius of rhabdomere	$\sim 0.5 \Delta x\, N_{micro,row}$
$V_{m,i}$	$2.34 \cdot 10^{-3}$	μm^3	Volume of microvillus	$\pi r_{m,i}^2 L_m$
S_m	0.18	μm^2	Membrane surface area of microvillus	$2\pi r_{m,i} L_m$
f_m	0.2	-	Extra-microvillus – microvillus lumen ratio	$1 - \pi r_{m,o}^2 / (\Delta x \Delta y)$
$V_{m,o}$	$0.47 \cdot 10^{-3}$	μm^3	Extra-microvillus volume	$f_m\, V_{m,i}$
Δx	74	nm	Spacing of microvilli between columns	(4)
Δy	48	nm	Spacing of microvilli between rows	(4)
N_{micro}	$35 \cdot 10^3$	-	Number of microvilli per rhabdomere	
$N_{micro,row}$	21	-	Number of microvilli per rhabdomere row	
$N_{micro,column}$	1667	-	Number of microvilli per rhabdomere column	
L_{cell}	80	µm	Length of photoreceptor cell	$\Delta y\, N_{micro,column}$
V_{cb}	1.01	pl	Volume of cell body	$(\pi r_{om}^2 - \pi r_{ic}^2) L_{cell} / N_{cell}$
V_{rh}	0.08	pl	Volume of rhabdomere	$V_{m,i}\, N_{micro}$
V_{ic}	0.91	pl	Volume of intra-ommatidial cavity	$(\pi r_{ic}^2 - N_{cell} \pi r_{rh}^2) L_{cell}$
$V_{ic,eff}$	0.52	pl	Effective volume of intra-ommatidial cavity	See text

With a single flash all photoreceptors in a single ommatidium will be activated. As a consequence the other photoreceptors will also draw Ca^{2+} ions (and other ions) from the intra-ommatidial cavity and increase depletion. However, because the other photoreceptor cells are not voltage clamped, the currents will be much smaller in amplitude. The effective number of photoreceptor cells that participate in the light response is one of the parameters that determines the effective volume of the intra-ommatidial cavity $V_{ic,eff} = V_{ic} / N_{eff}$. The value used in the model is $N_{eff} = 1.75$, giving $V_{ic,eff} = 0.52$ pl. Apart from smaller responses in the

non voltage-clamped cells, the values could also be smaller if there are Ca^{2+} buffers present in the intra-ommatidial cavity.

Ionic currents and fluxes The ionic fluxes considered in the model are: fluxes through TRP and TRPL channels, fluxes associated with the Na^+/Ca^{2+} exchanger, ionic fluxes between the intra-ommatidial cavity and the bath solution and diffusional fluxes.

Light induced channel current The light dependent TRP and TRPL are assumed to be localized only in the rhabdomere and are permeable to the cations Ca^{2+}, Na^+, K^+ and Mg^{2+}, present under physiological conditions. During the measurements intracellular K^+ was replaced by Cs^+ to block the voltage dependent potassium channels. TRP and TRPL channels are approximately equally permeable to K^+ ions and Cs^+ ions ($P_{K^+}/P_{Cs^+} \approx 1$); we therefore did not explicitly model the Cs^+ ions but combined K^+ and Cs^+ ions into a single $[K^+] \rightarrow [K^+]+[Cs^+]$ ion pool and $I_{K^+} \rightarrow I_{K^+} + I_{Cs^+}$ ion current. The total light activated channel current $I_{ch,tot}$ ($C \cdot s^{-1}$) is then the sum of Ca^{2+}, Na^+, K^+ and Mg^{2+} ionic currents:

$$I_{ch,tot} = I_{ch,Ca^{2+}} + I_{ch,Mg^{2+}} + I_{ch,Na^+} + I_{ch,K^+} \qquad \text{(Eq. S1)}$$

As a first order approximation we assume that the TRP and TRPL channels are uniformly distributed over the length of the microvillus and are synchronously activated, i.e. the permeability is also spatially uniform over the time course of the response. Assuming the validity of the Goldman-Hodgkin-Katz (GHK) equation, the current $I_{ch,S}$ ($C \cdot s^{-1}$) carried by ion q is described by the following surface integral:

$$I_{ch,S} = N_{micro} P_m w_S z_S F \int_{S_m} f_S dS_m \qquad \text{(Eq. S2a)}$$

where f_S is defined as :

$$f_S = E \frac{z_S F}{RT} \frac{[S]_i - [S]_o e^{-\frac{z_S F}{RT}E}}{1 - e^{-\frac{z_S F}{RT}E}} \qquad \text{(Eq. S2b)}$$

The microvillus membrane surface area is denoted by S_m (m^2), P_m ($m \cdot s^{-1}$) denotes the apparent total permeability, $w_S = P_S / \sum_S P_S$ denotes the normalized permeability of ion S, such that $\sum_S w_S = 1$. The relative permeabilities were independently measured (5, 6). The extracellular and intracellular ion concentrations of ion S are denoted by $[S]_o$ (mM) and $[S]_i$ (mM) respectively, z_S denotes the charge of ion S, R ($J \cdot K^{-1} \cdot mol^{-1}$) denotes the gas constant, F ($C \cdot mol^{-1}$) denotes Faraday's constant, T (K) denotes the absolute temperature and E (V)

denotes the membrane potential.

Given a measured light current we can then estimate the apparent total permeability using the following equation:

$$P_m = \frac{I_{ch,tot}}{N_{micro} \sum_S w_S z_S F \int_{S_m} f_S dS_m} \quad \text{(Eq. S3)}$$

Once P_m is determined, the ionic flux density $j_{ch,S}$ ($mM \cdot m^{-2} \cdot s^{-1}$) and concentration change $J_{ch,S}$ ($mM \cdot s^{-1}$) associated with ion S can be calculated using the following equations:

$$j_{ch,S} = P_m w_S f_S$$
$$J_{ch,S} = r_{sv} j_{ch,S} \quad \text{(Eq. S4a,b)}$$

where r_{sv} denotes the surface to volume ratio.

Because the ionic concentrations change during the time course of the light response, the fractional current of ion S will in fact change over time and is therefore not a constant. We can however calculate the charge fraction $P_{f,S}$ that was carried by ion S by calculating the charge ratio using the following equation:

$$P_{f,S} = \frac{\int_0^\infty I_{ch,S}(t)dt}{\int_0^\infty I_{ch,tot}(t)dt} \quad \text{(Eq. S5)}$$

TABLE II: Parameters used in the calculation of the ionic currents

parameter	value	unit	description	ref.
E	-70	mV	Membrane holding potential	set
T	293.15	K	Absolute temperature	set
R	8.3144621	$J \cdot K^{-1} \cdot mol^{-1}$	Gas constant	
F	96485.3365	$C \cdot mol^{-1}$	Faraday's constant	
$I_{light,tot}$	variable	$C \cdot s^{-1}$	Total light induced current	measured
I_S	variable	$C \cdot s^{-1}$	Light induced current of ion S	measured

parameter	Ca^{2+}	Mg^{2+}	Na^+	K^+	unit	description
z_s	2	2	1	1	-	charge
$[S]_o$	*variable*	4.0	120.0	5.0	mM	Initial concentration (as in bath)
$[S]_i$	*variable*	2.0	4	140.0	mM	Initial concentration (as in pipette)*
$w_{TRP,S}$	0.7566	0.2097	0.0169	0.0169	-	Normalized permeability for TRP channels
$w_{TRPL,S}$	0.5827	0.1897	0.1138	0.1138	-	Normalized permeability for TRPL channels
$w_{WT,S}$	0.7748	0.1600	0.0326	0.0326	-	Normalized permeability for WT

* Calculated using the Ca^{2+} equilibrium concentration predicted with Eq. S6b

In the measurements the extracellular Ca^{2+} concentrations were varied with values 0.75, 1.5, 3 and 10 mM and were used as extracellular starting concentrations. We assumed that at the start of each simulation the exchanger was in steady state, we therefore obtained the starting intracellular Ca^{2+} concentrations from the steady state exchanger concentration as described in Eq. S6b.

Exchanger current

After influx, Ca^{2+} ions are extruded in exchange for Na^+ ions by the Na^+/Ca^{2+} exchanger in a concentration and voltage dependent manner. We assume that the Na^+/Ca^{2+} exchanger is only located in the rhabdomeric membrane and that the distribution of Na^+/Ca^{2+} changer molecules is uniformly distributed along the length of the microvillus.

The exchanger is a complex protein comprising multiple regulatory and transport binding sites for $[Na^+]_o$, $[Na^+]_i$, $[Ca^{2+}]_o$ and $[Ca^{2+}]_i$ (7). Although for other organisms the mechanism and binding constants have been characterised in detail (e.g. 8), they have not yet been fully characterized for the *Drosophila* Na^+/Ca^{2+} exchanger CalX. For simplicity, we reduced the complexity of the Na^+/Ca^{2+} exchanger model using the following two minimal requirements: firstly, the exchanger current will saturate for high $[Ca^{2+}]_i$, and secondly given a certain membrane potential it should approach the correct equilibrium concentrations for $[Na^+]_o$, $[Na^+]_i$, $[Ca^{2+}]_o$ and $[Ca^{2+}]_i$, The exchanger current flux density i_X ($C \cdot m^{-2} \cdot s^{-1}$) is then described by the following sigmoid function:

$$i_X = Fk_X(t)\frac{\left[Ca^{2+}\right]_{i,eq} - \left[Ca^{2+}\right]_i}{K_X + \left[Ca^{2+}\right]_i} \qquad \text{(Eq. S6a)}$$

Where F denotes Faraday's constant, k_X ($mol \cdot m^{-2} \cdot s^{-1}$) denotes the maximal exchanger rate constant K_X (mM) denotes the concentration of half maximal exchanger current and $\left[Ca^{2+}\right]_{i,eq}$ denotes the equilibrium intracellular Ca^{2+} concentration, calculated using the following equation:

$$\left[Ca^{2+}\right]_{i,eq} = \left[Ca^{2+}\right]_o \left(\frac{\left[Na^+\right]_i}{\left[Na^+\right]_o}\right)^3 e^{\frac{FE}{RT}} \qquad \text{(Eq. S6b)}$$

In more complex models the kinetic parameters k_X and K_X may also depend on $[Na^+]_o$, $[Na^+]_i$, $[Ca^{2+}]_o$ and the membrane potential E. However, we measured the light induced currents under voltage clamp conditions; furthermore compared to the massive changes in $[Ca^{2+}]_i$, the concentration changes of $[Na^+]_o$, $[Na^+]_i$, $[Ca^{2+}]_o$ are relatively small. The kinetic parameters

k_X and K_X are therefore not expected to change considerably during the light response. The exchanger flux density $j_{X,S}$ and concentration change $J_{X,S}$ for Ca^{2+} and Na^+ can then be calculated using the following equations:

$$j_{X,S} = c_{X,Ss}\frac{i_X}{F}$$
$$J_{X,S} = r_{sv} j_{X,S} \qquad \text{(Eq. S7a, b)}$$

where $c_{X,S}$ denotes the exchanger coupling constant for ion *S* and r_{sv} denotes the surface to volume ratio.

The exchanger rate constant was tuned in such a way that the maximum total exchanger current is in the order of $k_X F S_m N_{micro}$ = 200 pA, which is the maximal exchanger currents measured in *Drosophila* fly photoreceptor cells (this study and 9) and fits the tail current just after the light response peak. The apparent Ca^{2+} concentration of half maximal exchanger current has not been measured directly and has been tuned in the model to get a reasonably good fit to the tail current and peak Ca^{2+} concentration in the rhabdomere. The value also depends on the Ca^{2+} concentrations reached in the cell-body, which in turn are dependent on calcium buffering.

TABLE III: Parameters used for the exchanger current.

parameter	value	unit	Description	ref.
k_X	$0.33\cdot10^{-6}$	$mol\cdot m^{-2}\cdot s^{-1}$	Exchanger rate constant	See text
K_X	30	µM	Concentration of half maximal exchanger current	Tuned
$c_{X,Ca^{2+}}$	1	-	Exchanger coupling constant for Ca^{2+}	
c_{X,Na^+}	-3	-	Exchanger coupling constant for Na^+	
$I_{X,max}$	200	pA	Maximal exchanger current	$k_X F S_m N_{micro}$

Diffusion between the intra-ommatidial cavity and the bath solution

The light-induced currents were measured in dissociated ommatidia in a bath solution. The ions in the intra-ommatidial cavity and the bath solution are assumed to exchange through passive diffusion. The flux $J_{ic\text{-}bath,S}$ ($mM\cdot s^{-1}$) of ions between the intra-ommatidial cavity and the bath solution can then be approximated by the following diffusion equation:

$$J_{ic-bath,S} = D_{S,o}\frac{A_{ic-bath}}{V_{ic}L_{ic-bath}}\left([S]_{bath}-[S]_{ic}\right) = D_{S,o}g_{ic-bath}\left([S]_{bath}-[S]_{ic}\right) = \frac{[S]_{bath}-[S]_{ic}}{\tau_{S,ic}} \quad \text{(Eq. S8)}$$

where $A_{ic\text{-}bath}$ (m^2) denotes the effective cross sectional area through which the flux occurs, V_{ic} (m^3) denotes the intra-ommatidial volume, $L_{ic\text{-}bath}$ (m) denotes the effective diffusion path length and $g_{ic\text{-}bath} = A_{ic\text{-}bath} / (V_{ic}\, L_{ic\text{-}bath})$ (m^2) denotes the combined geometry parameter. The time constant $\tau_{S,ic} = 1/\left(D_{S,o}g_{ic-bath}\right)$ (s) only depends on the extracellular diffusion coefficient and the geometry parameter.

The geometrical parameter $g_{ic\text{-}bath}$ cannot easily be measured directly; however, based on the measurement of exchanger currents during bath solution changes (10) the time constant for Na^+ is estimated to be about $\tau_{Na^+,ic}$ = 100 ms. From this and assuming that the geometry parameter is the same for each ion, the time constants of other ions can be estimated with the following equation:

$$\tau_{S,ic} = \frac{D_{Na^+,o}}{D_{S,o}}\tau_{Na^+,ic} \quad \text{(Eq. S9)}$$

TABLE IV: Time constants for fluxes between intra-ommatidial cavity and bath solution.

parameter	value	unit	description	reference
$\tau_{Ca^{2+},ic}$	200	ms	Intra-ommatidial Ca^{2+} time constant	$\tau_{Ca^{2+},ic} = \tau_{Na^+,ic} D_{Na^+,o} / D_{Ca^{2+},o}$
$\tau_{Mg^{2+},ic}$	225	ms	Intra-ommatidial Mg^{2+} time constant	$\tau_{Mg^{2+},ic} = \tau_{Na^+,ic} D_{Na^+,o} / D_{Mg^{2+},o}$
$\tau_{Na^+,ic}$	100	ms	Intra-ommatidial Na^+ time constant	See text
$\tau_{K^+,ic}$	70	ms	Intra-ommatidial K^+ time constant	$\tau_{K^+,ic} = \tau_{Na^+,ic} D_{Na^+,o} / D_{K^+,o}$

Diffusion of ions

Ions are assumed to diffuse in the microvillus, the cell-body and the extra-microvillar space. Mobilities of ions in the cytoplasm compared to water are generally 1.5-2 fold lower because of the higher viscosity of the cytoplasm (11). The mobility of Ca^{2+} is even further reduced because of binding to non-specific negatively charged structures. The diffusion coefficients of the different ions have not been measured directly in fly photoreceptors; we therefore use

values measured in other cell types (Table V). We also assume that the viscosity of the fluid in the extracellular space is similar to water and therefore used diffusion coefficients measured in water. Because of the higher viscosity, we assume that the cytoplasmic Mg^{2+} diffusion coefficient is about twofold lower than the Mg^{2+} diffusion coefficient in water, hence $D_{Mg^{2+},i} = 285\ \mu m^2 \cdot s^{-1}$. The cytoplasmic Mg^{2+} diffusion coefficient could even be lower $D_{Mg^{2+},i} = 200\ \mu m^2 \cdot s^{-1}$ if Mg^{2+}, like Ca^{2+}, also binds to negatively charged structures (2).

TABLE V: Diffusion coefficients used in the simulations

parameter	value	unit	description	reference
$D_{Ca^{2+},i}$	220	$\mu m^2 \cdot s^{-1}$	Cell body Ca^{2+} diffusion coefficient	(12)
$D_{Mga^{2+},i}$	285	$\mu m^2 \cdot s^{-1}$	Intracellular Mg^{2+} diffusion coefficient	See text
$D_{Na^{+},i}$	650	$\mu m^2 \cdot s^{-1}$	Intracellular Na^{+} diffusion coefficient	(11)
$D_{K^{2+},i}$	1000	$\mu m^2 \cdot s^{-1}$	Intracellular K^{+} diffusion coefficient	(11)
$D_{Ca^{2+},o}$	650	$\mu m^2 \cdot s^{-1}$	Extracellular Ca^{2+} diffusion coefficient	(11)
$D_{Mg^{2+},o}$	575	$\mu m^2 \cdot s^{-1}$	Extracellular Mg^{2+} diffusion coefficient	(13)
$D_{Na^{+},o}$	1300	$\mu m^2 \cdot s^{-1}$	Extracellular Na^{+} diffusion coefficient	(11)
$D_{K^{+},o}$	1800	$\mu m^2 \cdot s^{-1}$	Extracellular K^{+} diffusion coefficient	(11)

Calcium buffers

Ca^{2+} ions are buffered by several Ca^{2+} binding proteins and negatively charged lipids, which will affect the kinetics and also the magnitude of Ca^{2+} concentration changes. In general the kinetics, i.e. diffusion and fluxes, slows down when calcium buffers are immobile and the magnitude of concentration changes will be smaller. The photoreceptor cell constitutes several known specific calcium binding proteins including calmodulin (14), calphotin (15-17) and calnexin (18) . Furthermore, non-specific calcium binding molecules such as negatively charged membrane lipids are present.

In most cases binding and unbinding of Ca^{2+} ions is relatively fast. We therefore assume that buffering of Ca^{2+} ions occurs instantaneously, which allows the effect of Ca^{2+}

buffers to be described by a buffering power factor. The total buffering power can be directly obtained from the binding equations by taking the first derivative:

$$\begin{aligned}\beta_{tot,Ca^{2+}} &= 1 + \sum_B \frac{\partial[B \cdot \mathrm{Ca}^{2+}]}{\partial[\mathrm{Ca}^{2+}]} \\ &= 1 + \sum_B \beta_{B,\mathrm{Ca}^{2+}}\end{aligned} \qquad \text{(Eq. S10)}$$

Where $\beta_{B,\mathrm{Ca}^{2+}} = \partial[B \cdot \mathrm{Ca}^{2+}] / \partial[\mathrm{Ca}^{2+}]$ denotes the Ca^{2+} buffering for buffer *B*.

Calmodulin

Calmodulin is a high affinity low capacity calcium binding protein containing four Ca^{2+} binding sites. Calmodulin is enriched in the rhabdomere, where it binds TRP, TRPL, NINAC and INAD molecules and is also present in the cell body at lower concentration levels. The calcium bound calmodulin concentration is assumed to follow the Adair-Klotz equation (19):

$$[\mathrm{cam} \cdot \mathrm{Ca}^{2+}] = [\mathrm{cam}]_{tot} \frac{K_1[\mathrm{Ca}^{2+}] + 2K_1K_2[\mathrm{Ca}^{2+}]^2 + 3K_1K_2K_3[\mathrm{Ca}^{2+}]^3 + 4K_1K_2K_3K_4[\mathrm{Ca}^{2+}]^4}{1 + K_1[\mathrm{Ca}^{2+}] + K_1K_2[\mathrm{Ca}^{2+}]^2 + K_1K_2K_3[\mathrm{Ca}^{2+}]^3 + K_1K_2K_3K_4[\mathrm{Ca}^{2+}]^4} \qquad \text{(Eq. S11a)}$$

where K_1, K_2, K_3 and K_4 denote the macroscopic binding constants of the four binding sites, and $[Ca^{2+}]$ denotes the free Ca^{2+} concentration. For *Drosophila* these have been estimated to be 800, 200, 70 and 40 mM^{-1} respectively (19). $[cam]_{tot}$ denotes the total, bound and unbound, calmodulin concentration. This is estimated to be about $[cam]_m$ = 0.5 mM in the rhabdomere and $[cam]_{cb}$ = 0.025 mM in the cell-body (14). We assume that calmodulin is effectively immobile.

By taking the first derivative $[\mathrm{cam} \cdot \mathrm{Ca}^{2+}]$, we obtain the following equation for the buffering power associated with calmodulin:

$$\beta_{cam,Ca^{2+}} = \frac{dN \cdot D - N \cdot dD}{D^2} \qquad \text{(Eq. S11b)}$$

where *N*, *dN*, *D*, and *dD* are defined as:

$$\begin{aligned} N &= K_1[\mathrm{Ca}^{2+}] + 2K_1K_2[\mathrm{Ca}^{2+}]^2 + 3K_1K_2K_3[\mathrm{Ca}^{2+}]^3 + 4K_1K_2K_3K_4[\mathrm{Ca}^{2+}]^4 \\ dN &= K_1 + 4K_1K_2[\mathrm{Ca}^{2+}] + 9K_1K_2K_3[\mathrm{Ca}^{2+}]^2 + 16K_1K_2K_3K_4[\mathrm{Ca}^{2+}]^3 \\ D &= 1 + K_1[\mathrm{Ca}^{2+}] + K_1K_2[\mathrm{Ca}^{2+}]^2 + K_1K_2K_3[\mathrm{Ca}^{2+}]^3 + K_1K_2K_3K_4[\mathrm{Ca}^{2+}]^4 \\ dD &= K_1 + 2K_1K_2[\mathrm{Ca}^{2+}] + 3K_1K_2K_3[\mathrm{Ca}^{2+}]^2 + 4K_1K_2K_3K_4[\mathrm{Ca}^{2+}]^3 \end{aligned} \qquad \text{(Eq. S11c-f)}$$

TABLE VI: Calmodulin Ca^{2+} binding parameters

parameter	value	unit	description	ref.
$[\text{cam}]_m$	0.5	mM	Microvillar calmodulin concentration	(14)
$[\text{cam}]_{cb}$	0.025	mM	Cell-body calmodulin concentration	(14)
K_1	800	mM^{-1}	Calmodulin macroscopic Ca^{2+} binding constant	(19)
K_2	200	mM^{-1}	Calmodulin macroscopic Ca^{2+} binding constant	(19)
K_3	70	mM^{-1}	Calmodulin macroscopic Ca^{2+} binding constant	(19)
K_4	40	mM^{-1}	Calmodulin macroscopic Ca^{2+} binding constant	(19)

Negatively charged phospholipids

Negatively charged phospholipids can bind Ca^{2+} and Mg^{2+} ions (McLaughlin et al., 1981). The three dominant negatively charged phospholipids that contribute are phosphatidylethanolamine (PE), phosphatidylcholine (PC) and phosphatidylserine (PS) (20, 21). Because the surface to volume ratio for the microvillus lumen and extra-microvillus space is high, the effective concentration of these phospholipids is high (2, 22). Although the affinity for Ca^{2+} is low, they can contribute to the buffering power because of the high effective concentrations.

At steady state the competitive binding of Ca^{2+} to phospholipid PL can be approximated by the following binding equation:

$$\left[\mathbf{PL}\cdot\mathbf{Ca}^{2+}\right]=\left[\mathbf{PL}\right]_{tot}\frac{\left[\mathbf{Ca}^{2+}\right]}{K_{PL,\mathbf{Ca}^{2+}}+\left[\mathbf{Ca}^{2+}\right]} \qquad \text{(Eq. S12a)}$$

Where $[PL\cdot Ca^{2+}]$ denotes the bound concentration of Ca^{2+}, $[PL]_{tot}$ denotes the total bound and unbound phospholipid concentration, $K_{PL,Ca^{2+}}$ denotes the dissociation constants of Ca^{2+}

The corresponding buffering power equation for Ca^{2+} is:

$$\beta_{PL,Ca^{2+}}=\left[\mathbf{PL}\right]_{tot}\frac{K_{PL,\mathbf{Ca}^{2+}}}{\left(K_{PL,\mathbf{Ca}^{2+}}+\left[\mathbf{Ca}^{2+}\right]\right)^2} \qquad \text{(Eq. S12b)}$$

TABLE VII: Phospholipid concentrations and Ca^{2+} binding parameters.

parameter	value	unit	description	ref.
$[PE]_{tot,m,i}$	80	mM	Microvillar PE concentration	(2)
$[PC]_{tot,m,i}$	40	mM	Microvillar PC concentration	(2)
$[PS]_{tot,m,i}$	8	mM	Microvillar PS concentration	(2)
$[PE]_{tot,m,o}$	400	mM	Extra-microvillar PE concentration	
$[PC]_{tot,m,o}$	200	mM	Extra-microvillar PC concentration	
$[PS]_{tot,m,o}$	40	mM	Extra-microvillar PS concentration	
$K_{PE,Ca^{2+}}$	333.3	mM	PE Ca^{2+} dissociation constant	(22)
$K_{PC,Ca^{2+}}$	333.3	mM	PC Ca^{2+} dissociation constant	(22)
$K_{PS,Ca^{2+}}$	83.3	mM	PS Ca^{2+} dissociation constant	(22)

Cell body calcium buffers

Two immobile high capacity low affinity calcium binding proteins have been reported in fly photoreceptor cells. First, calphotin, which is localized in a band in the cell body at the base of the rhabdomere (15-17) and secondly, calnexin, which is assumed to be localized in the region of the cell body that does not contain calphotin (18) The concentration of calphotin and calnexin, and their affinities for calcium ions have not been measured directly. We therefore tuned these parameters in such a way that we get more or less the correct peak Ca^{2+} concentration after a strong light flash. Calphotin was attributed a higher concentration as mutant analysis indicates it is the more important of the two buffers (17, 18). Using calcium indicators, the peak average Ca^{2+} concentration in the cell body has been estimated to reach values in the order of 50 μM (23). For calphotin and calnexin we use the following simple binding equations:

$$[\mathrm{cpn}\cdot\mathrm{Ca}^{2+}] = [\mathrm{cpn}]_{tot}\frac{[\mathrm{Ca}^{2+}]}{[\mathrm{Ca}^{2+}]+K_{cpn}} \qquad \text{(Eq. S13a)}$$

$$[\mathrm{cnx}\cdot\mathrm{Ca}^{2+}] = [\mathrm{cnx}]_{tot}\frac{[\mathrm{Ca}^{2+}]}{[\mathrm{Ca}^{2+}]+K_{cnx}} \qquad \text{(Eq. S14a)}$$

where K_{cpn} and K_{cnx} denote the dissociation constants of calphotin and calnexin respectively. The total, bound and unbound, calphotin and calnexin concentrations are denoted by $[cpn]_{tot}$

and $[cnx]_{tot}$ respectively. By taking the first derivative with respect to $[Ca^{2+}]$ we obtain the buffering power:

$$\beta_{cpn,Ca^{2+}} = [cpn]_{tot} \frac{K_{cpn}}{([Ca^{2+}] + K_{cpn})^2} \quad \text{(Eq. S13b)}$$

$$\beta_{cnx,Ca^{2+}} = [cnx]_{tot} \frac{K_{cpn}}{([Ca^{2+}] + K_{cnx})^2} \quad \text{(Eq. S14b)}$$

We have also included a low capacity high affinity Ca^{2+} buffer ($[B]_{cb}$), which is uniformly distributed throughout the cell-body, and partly accounts for slow Ca^{2+} extrusion at lower Ca^{2+} concentrations.

TABLE VIII: Cell-body Ca^{2+} buffers and binding parameters.

parameter	value	unit	description	ref.
$[cpn]_{cb}$	4*	mM	Average cell- body calphotin concentration	Tuned
K_{cpn}	1	mM	Calphotin Ca^{2+} dissociation constant	Tuned
w_{cpn}	1	µm	Width of calphotin expression band	
$[cnx]_{cb}$	1*	mM	Average cell- body calnexin concentration	Tuned
K_{cpn}	1	mM	Calnexin Ca^{2+} dissociation constant	Tuned
w_{cnx}	2.2	µm	Width of calnexin expression band	d_{cb}- w_{cpn}
$[B]_{cb}$	0.2	mM	Immobile cell body Ca^{2+} buffer	Tuned
K_{cb}	0.02	mM	Immobile cell body Ca^{2+} buffer dissociation constant	Tuned

*The local concentration of calphotin is 20.1 mM in the calphotin expression band, and the local concentration of calnexin 2.25 mM in the calnexin expression band.

Intracellular Ca^{2+} stores

Apart from Ca^{2+} buffers intracellular stores, including components of the ER and mitochondria can also contribute to Ca^{2+} homeostasis by uptake of excess Ca^{2+} and subsequent release after Ca^{2+} reduction (24). Furthermore, fly photoreceptor cells also contain mitochondria, which are mainly located at the distal part close to the basolateral membrane of the cell body. Although no direct experimental evidence exists for fly photoreceptors cells, it is well known from other cell types that mitochondria contribute to Ca^{2+} uptake, especially at higher levels of intracellular Ca^{2+} concentrations. It has been shown that mitochondria are readily activated upon light stimulation suggesting that take up Ca^{2+} after influx (25).

Although stores will contribute to Ca^{2+} dynamics, apart from peak amplitude, we do not expect they will have a significant effect on the time course of Ca^{2+} dynamics at the high levels of Ca^{2+} estimated in the experiments used in this study, and we found no effect of the SERC inhibitor thapsigargin on the CalX tail currents. Because little is known about Ca^{2+} dynamics in fly-photoreceptor mitochondria we have not included this in the current model.

Transport equations

For the intracellular space that spans the microvillus lumen, the neck, and the cell body we use the following flux-diffusion equation that describes the intracellular concentration changes:

$$\frac{\partial [S]_i}{\partial t} = \frac{1}{\beta_{tot,S,i}} \left(D_{S,i} \nabla^2 [S]_i + J_{S,i} \right) \qquad \text{(Eq. S15a)}$$

Where $J_{S,i}$ denotes the total flux of ions. For ions $S = \{Ca^{2+}, Na^{+}\}$ the total flux is:

$$\begin{aligned} J_{S,i} &= r_{sv,m} j_{ch,S} + r_{sv,m} j_{X,S} \quad && 0 \geq x \geq L_m \\ J_{S,i} &= 0 && L_m + L_n \geq x \geq L_m + L_n + d_{cb} \end{aligned} \qquad \text{(Eq. S15b, c)}$$

and for ions $S = \{Mg^{2+}, K^{+}\}$ the total flux is:

$$\begin{aligned} J_{S,i} &= r_{sv,m} j_{ch,S} \quad && 0 \geq x \geq L_m \\ J_{S,i} &= 0 && L_m + L_n \geq x \geq L_m + L_n + d_{cb} \end{aligned} \qquad \text{(Eq. S15d, e)}$$

The surface to volume ratio for the microvillus lumen is calculated from $r_{sv,m} = 2/r_{m,i}$. The buffering power $\beta_{tot,S,i} = 1$ for ions S = $\{Na^{+}, K^{+}\}$. We assume that the intracellular space is closed and therefore use the following boundary conditions:

$$\nabla [S]_i \big|_{x=0} = 0 \qquad \text{(Eq. S15f)}$$

$$\nabla [S]_i \big|_{x=L_m+L_n+d_{cb}} = 0 \qquad \text{(Eq. S15g)}$$

For the extra-microvillus space we use the following flux-diffusion equation that describes the extra-microvillus concentration changes:

$$\frac{\partial [S]_o}{\partial t} = \frac{1}{\beta_{tot,S,em}} \left(D_{S,o} \nabla^2 [S]_o + J_{S,em} \right) \qquad \text{(Eq. S16a)}$$

Where $J_{S,em}$ denotes the total flux of ions in the extra-microvillus space. For ions $S = \{Ca^{2+}, Na^{+}\}$ the total flux is:

$$J_{S,o} = -r_{sv,em} j_{ch,S} - r_{sv,em} j_{X,S} \quad 0 \geq x \geq L_m + L_n \qquad \text{(Eq. S16b)}$$

And for ions $S = \{Mg^{2+}, K^{+}\}$ the total flux is:

$$J_{S,o} = -r_{sv,em} j_{ch,S} \quad 0 \geq x \geq L_m + L_n \qquad \text{(Eq. S16c)}$$

The surface to volume ratio for the microvillus lumen is calculated from $r_{sv,em} = 2/(r_{m,i} f_m)$. The buffering power $\beta_{tot,S,em} = 1$ for ions $S = \{Na^+, K^+\}$. We assumed that the intracellular space is closed at the base of the microvilli and open at the tip of the microvilli, this yields the following boundary conditions:

$$\nabla[S]_i\big|_{x=L_m} = 0 \qquad \text{(Eq. S16d)}$$

$$[S]_o\big|_{x=0} = [S]_{ic} \qquad \text{(Eq. S16e)}$$

Where $[S]_{ic}$ denotes the concentration of ion S in the intra-ommatidial cavity. For the concentration changes in the intra-ommatidial cavity we use the following flux-equation:

$$\frac{\partial [S]_{ic}}{\partial t} = \frac{1}{\beta_{tot,S,ic}} \left(N_{cell} J_{ic-em,S} + J_{ic-bath,S} \right) \qquad \text{(Eq. S17)}$$

where N_{cell} denotes the effective number of cells that participate in the light response. In principle all seven photoreceptor cells will be activated by the light flash and will lead to ion concentration changes in the intra-ommatidial cavity. However, the voltage-clamped cell will generate stronger fluxes because the change in membrane voltage reduces the driving force for ions in the other six photoreceptor cells. The flux of ions between the extra-microvillus space and the intra-ommatidial cavity at the tip of the microvilli is denoted by $J_{ic\text{-}em,S}$:

$$J_{ic-em,S} = D_{S,o} \frac{A_{ic-em}}{V_{ic}} \nabla[S]_o\Big|_{x=0} \qquad \text{(Eq. S18)}$$

where $A_{ic-em} = f_m \pi r_m^2$ is the cross-sectional area of the extra-microvillus space. The buffering power $\beta_{tot,S,ic} = 1$ for ions $S = \{Ca^{2+}, Mg^{2+}, Na^+, K^+\}$.

Implementation

We used a finite volume scheme to discretize the diffusion operator, where we used Cartesian coordinates for the microvillus lumen and the extra-microvillus space (18 compartments). For the cell body we used polar coordinates (10 compartments). At the transition of the microvillus and cell body the volumes of the last compartment of the microvillus and first compartment of the cell-body were corrected for the volume of the neck. The cross sectional area of the neck was used to connect the two compartments. The light activated channel current between measurement time points $\{t_n, t_{n+1}\}$ was calculated using linear interpolation:

$$I_{ch,tot}(t) = I_{ch,tot}(t_n) + \frac{I_{ch,tot}(t_{n+1}) - I_{ch,tot}(t_n)}{t_{n+1} - t_n} (t_{n+1} - t) \qquad \text{(Eq. S19)}$$

The transport equations were numerically integrated using the forward Euler scheme. The model was implemented in C++ and compiled as a Matlab mex-function.

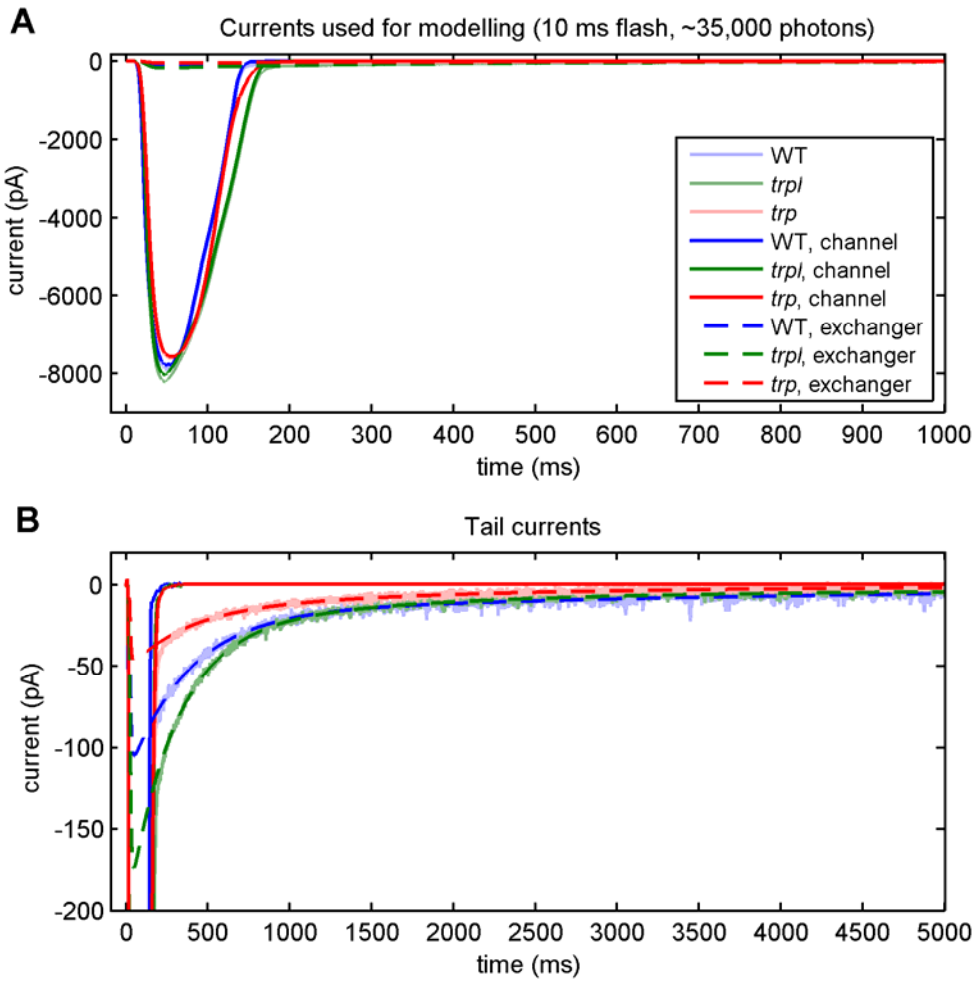

FIGURE S2: WT, *trpl*, and *trp* traces used for modelling. (*A*) The light induced currents in response to a 10 ms flash measured in $[Ca^{2+}]_o$ = 1.5 mM. The intensity was equivalent to ~35,000 effectively absorbed photons, on average activating one rhodopsin in each microvillus of the rhabdomere. (*B*) the light induced current (I_{tot}) was separated into a channel current and an exchanger current. The tail current was fitted with a double exponential function (WT: τ_{fast} = 363 ms, τ_{slow} = 3622 ms; *trpl*: τ_{fast} = 279 ms, τ_{slow} = 1462 ms; *trp*: τ_{fast} = 336 ms, τ_{slow} = 1600 ms), which was subsequently smoothly clipped up to about 25 ms (1). An estimate of the current associated with the channels ($I_{ch,tot}$), which was used as an input for the simulations was obtained by subtracting the estimated exchanger current (I_X) from the measured light induced current.

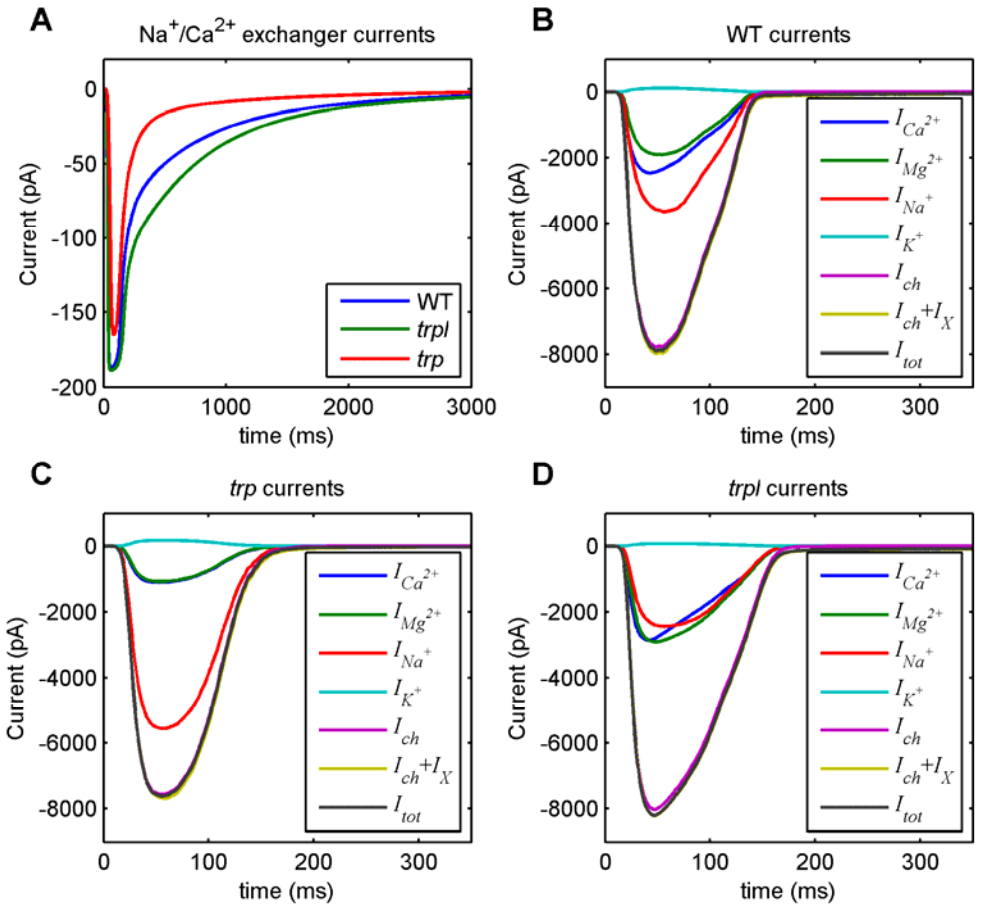

FIGURE S3: Simulated exchanger (*A*) and ionic currents for WT (*B*), *trp* (*C*), and *trpl* (*D*). The exchanger current saturates close to maximum values during the peak of the light induced current. The tail current of the exchanger decays exponentially while Ca^{2+} ions are extruded from the cell. While Ca^{2+}, Mg^{2+} and Na^+ contribute more or less equally in *trpl* flies, the Na^+ current is the largest light-induced current in *trp* and WT flies. I_{ch} denotes the estimated channel current (tail current subtracted), I_X denotes the modelled exchanger current, I_{tot} denotes the measured light-induced current (LIC).

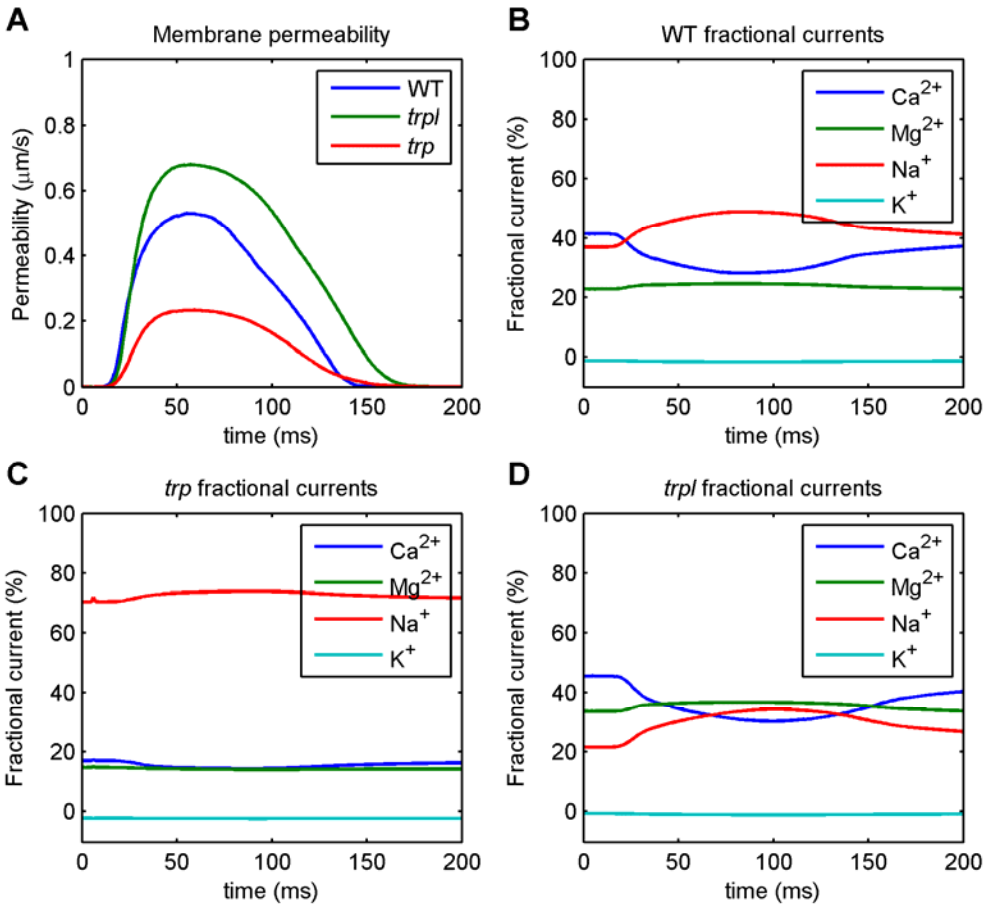

FIGURE S4: Apparent channel permeability for WT, *trp*, and *trpl*. (*A*) The permeability is highest for *trpl* flies and lowest for *trp* flies, while WT flies show an intermediate permeability. (*B-D*) show the time course of the fractional current of the different ions for WT, *trp*, and *trpl* For WT and *trpl* flies the fractional currents of Ca^{2+} decrease significantly, while the fractional currents of Mg^{2+} and Na^{+} increase significantly. The fractional current of K^{+} is hardly affected.

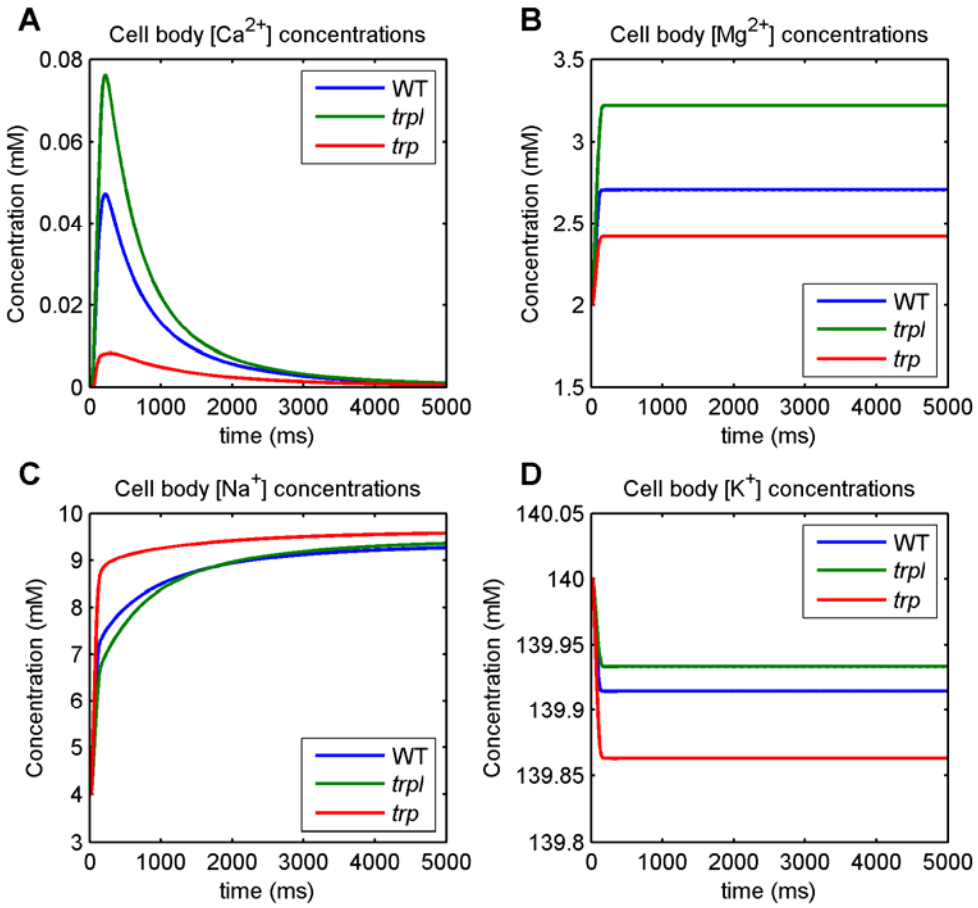

FIGURE S5: Simulated spatially averaged ionic concentrations in the cell body. (*A*) Ca^{2+} concentrations peak around ~200 ms, after which the exchanger extrudes the Ca^{2+} ions from the cell in exchange for Na^{+} ions. WT flies show a peak cell body Ca^{2+} concentration of about 50 µM, *trpl* flies, with a higher Ca^{2+} permeability show a peak cell body Ca^{2+} concentration of about 75 µM. The less Ca^{2+} permeable *trp* flies show a lower peak cell body Ca^{2+} concentration of about 10 µM. (*B*) Cell body Mg^{2+} concentrations show a rapid increase before reaching a steady-state level. (*C*) Cell body Na^{+} concentrations show a fast increase during the peak light current, after which they further increase due to the action of the Na^{+}/Ca^{2+} exchanger. (*D*) Cell body K^{+} concentrations show a very small fast decrease during the peak light response, after which they reach steady state levels. Mg^{2+} Na^{+} and K^{+} concentration do not change further over longer times because the Na^{+}/K^{+} pump was blocked in the simulation (as it was during the measurements) and because Mg^{2+} extrusion was not modelled.

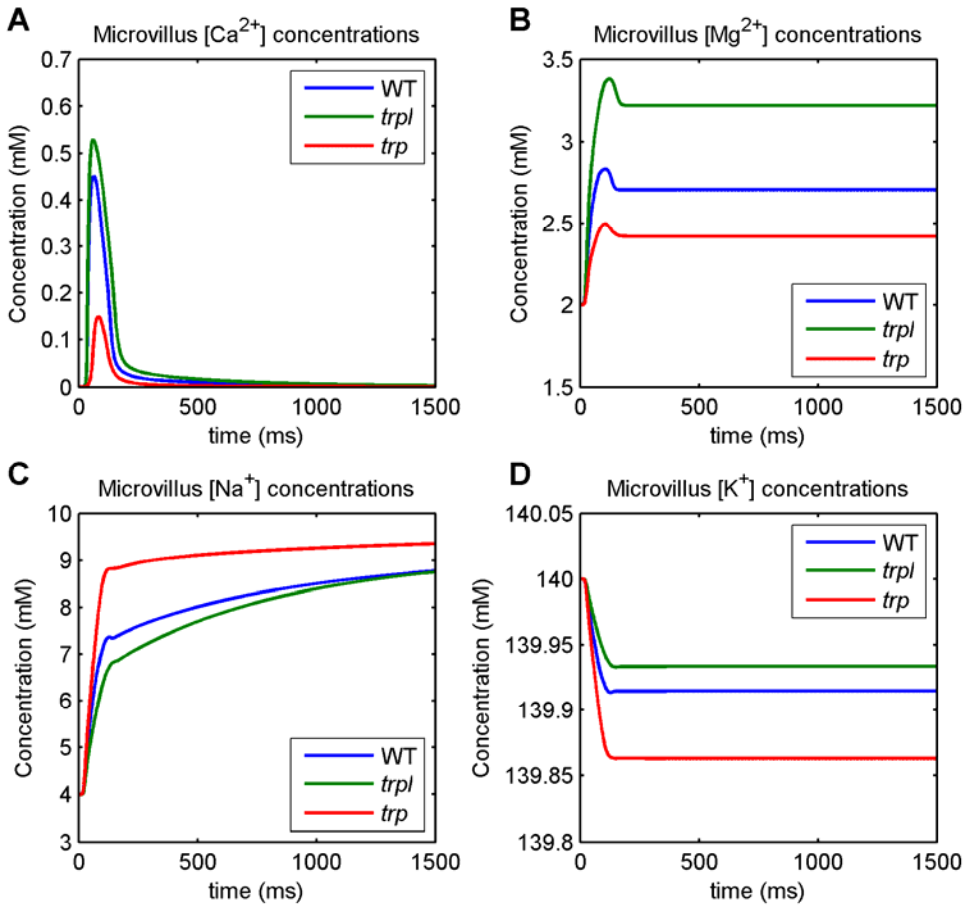

FIGURE S6: Simulated spatially averaged ionic concentrations in the microvillus. (*A*) Ca^{2+} concentrations show an initial steep rise reaching 150, 450 and 520 µM for *trp*, WT and *trpl* flies respectively, after which the concentrations decrease mainly due to diffusion into the cell body. During and after the peak light current the Na^{+}/Ca^{2+} exchanger extrudes Ca^{2+} ions from the cell in exchange of Na^{+} ions. (*B*) Mg^{2+} shows a steep rise with a small transient peak, which disappears when Mg^{2+} ions diffuse from the microvillus into the cell body and reaches steady state (*C*) After a steep rise Na^{+} concentrations slowly increase while the exchanger extrudes Ca^{2+} ions. (*D*) K^{+} concentrations show a small decrease, after which they equilibrate with the cell body.

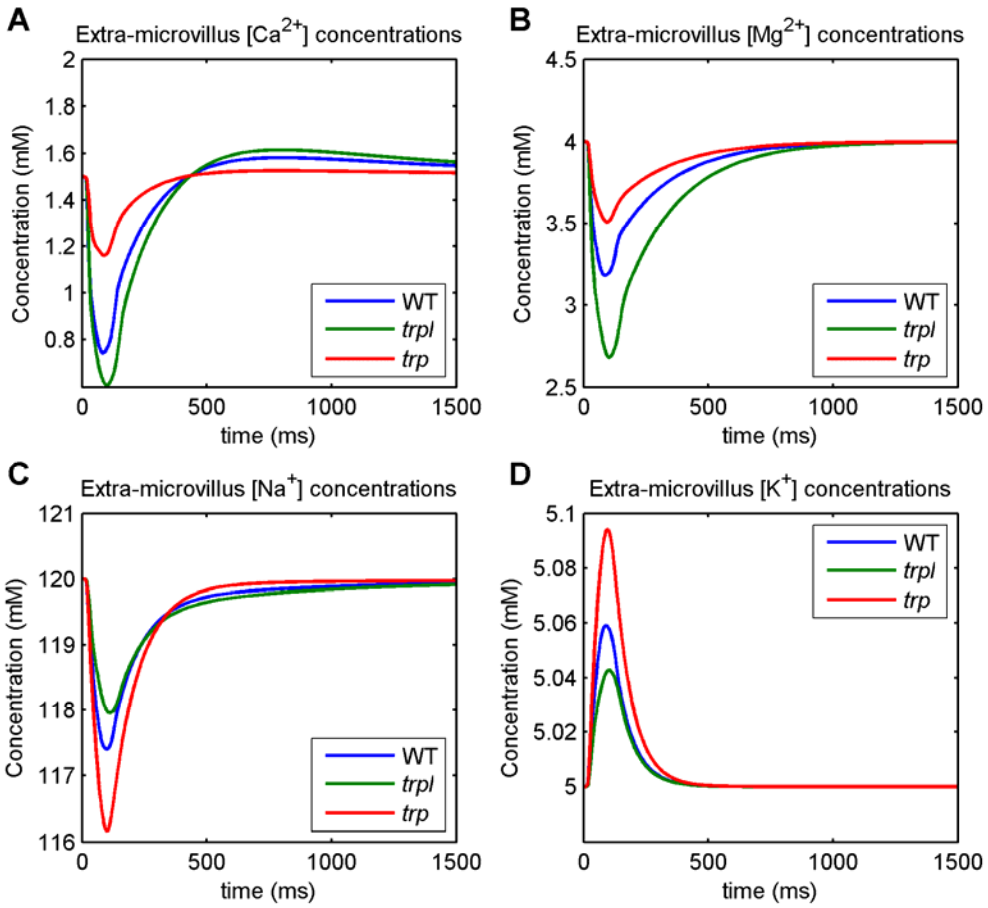

FIGURE S7: Simulated spatially averaged ionic concentrations in the extra-microvillus space. (*A*) Ca^{2+} concentrations of *trpl* and WT flies show a significant depletion in the extra-microvillus space during the peak light current, which will reduce the relative influx of Ca^{2+} ions during the light response. For *trp* flies the depletion is less pronounced and will have a smaller effect on the influx of Ca^{2+} ions. (*B*) Mg^{2+} shows a similar decrease compared to Ca^{2+} concentrations. (*C*) Na^{+} ions are also depleted, but the relative change is negligible (~5%). (*D*) K^{+} ion concentrations are almost unaffected. Diffusional recovery from the intra-ommatidial cavity and bath solution cannot keep up with massive flux of ions through the channels from the extra-microvillus space into the microvillus, which causes the observed transient depletion.

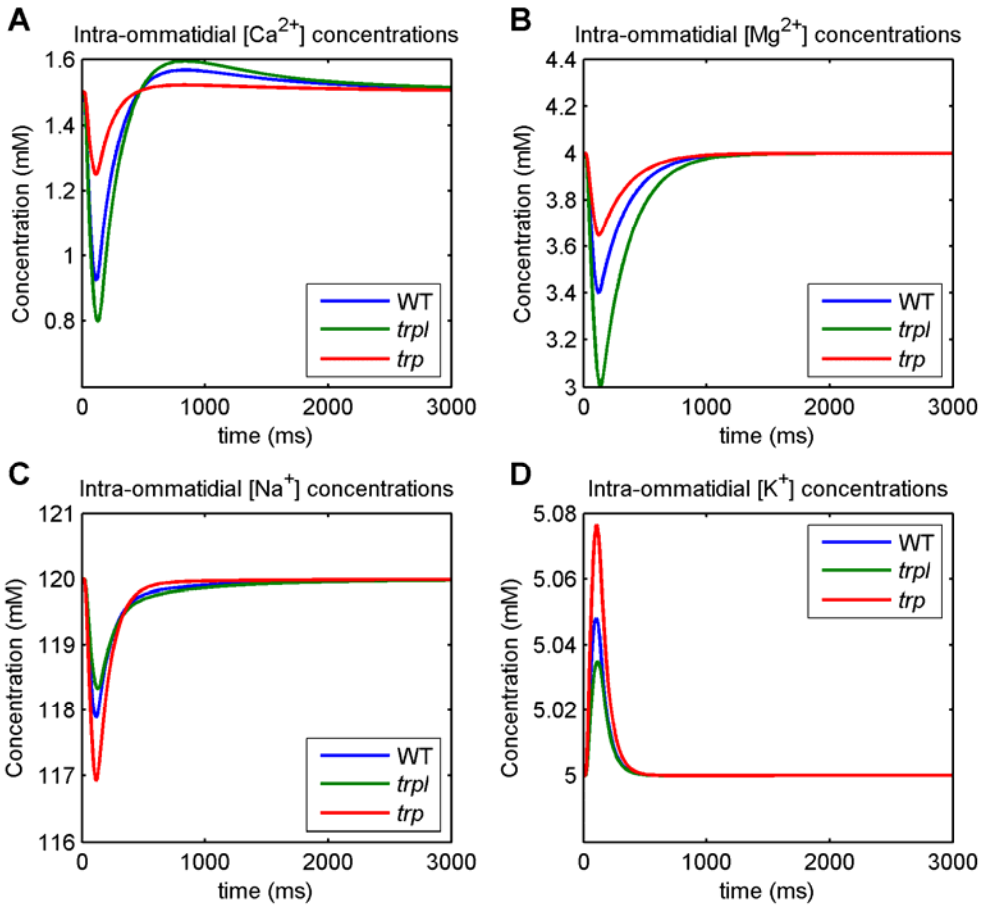

FIGURE S8: Simulated spatially averaged ionic concentrations in the intra-ommatidial cavity. The ionic concentration changes in the intra-ommatidial cavity are similar to those in the extra-microvillus space, however they are less pronounced. The extra-microvillus space is spatially more constricted and has a smaller volume than the intra-ommatidial cavity. (*A*) Ca^{2+} concentrations show an overshoot after the peak light current, which is caused by recovery of Ca^{2+} concentrations from the bath solution, during which the exchanger has not yet reached steady state and continues to extrude Ca^{2+} into the extracellular space. Because of diffusional recovery from the bath solution all ionic concentrations ultimately will reach the bath solution concentration. The effective number of photoreceptor cells that participate in the light response has a marked effect on the level of depletion. The Ca^{2+} concentrations obtained with N_{eff} = 1.75 are more in line with previously reported values (26) and also give fractional Ca^{2+} currents that are close to the measured values. The Ca^{2+} concentrations in the cell body are however higher and give a poorer agreement with the tail current. The influx of Ca^{2+} can be reduced by allowing more depletion in the extracellular space, which can be achieved by taking N_{eff} = 2. Although the tail currents are well fitted now the decrease in Ca^{2+} concentrations in the intra-ommatidial cavity is to strong, which has the effect of reducing the fractional Ca^{2+} current more than measured.

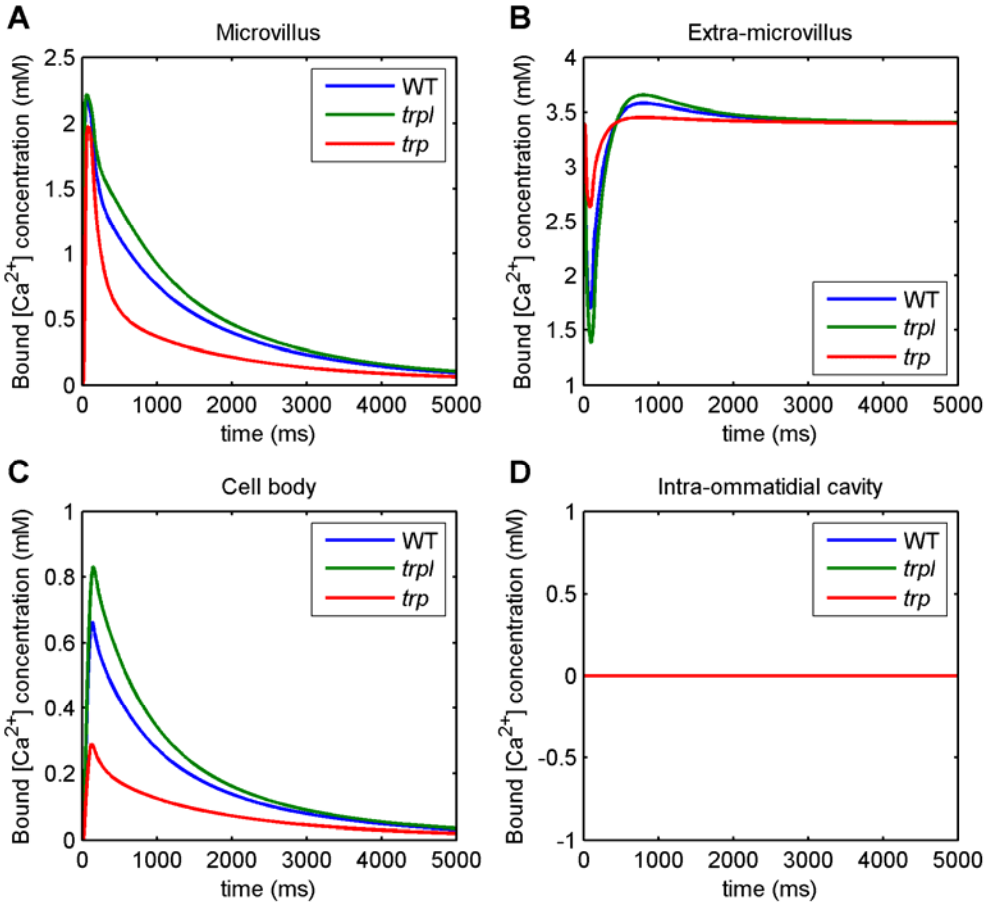

FIGURE S9: Spatially averaged concentrations of bound Ca^{2+} ions in the different compartments (*A-D*). Calmodulin is the main Ca^{2+} buffer in the microvillus and is saturated during the peak of the light current. Phospholipids in the extra-microvillus space mainly contribute to buffering, and in the cell body a low concentration of calmodulin and high capacity low affinity buffers (calphotin and calnexin) bind Ca^{2+} ions. The latter are necessary to reduce the peak Ca^{2+} concentration in the cell body to correct range and also slow down diffusion of Ca^{2+} in the cell body. In these simulations it was assumed there were no Ca^{2+} buffers present in the intra-ommatidial cavity.

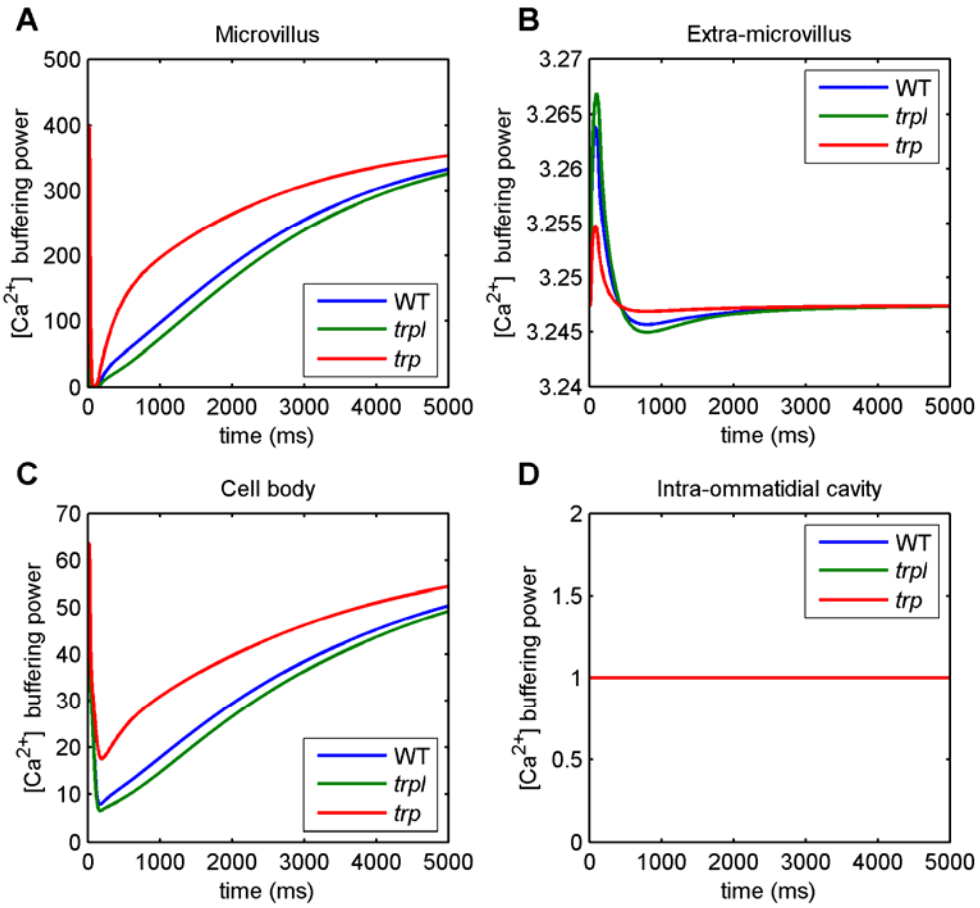

FIGURE S10: Spatially averaged Ca^{2+} buffering power as a result of Ca^{2+} buffers in the different compartments (*A-D*). At low Ca^{2+} concentrations calmodulin has a very high buffering power (400), which collapses almost completely during the peak light response when the microvillus is flooded with Ca^{2+} ions in effect saturating calmodulin. At high Ca^{2+} concentrations the buffering power in the cell body is dominated by calphotin and calnexin, while at low Ca^{2+} concentrations cell body calmodulin mainly determines the Ca^{2+} buffering power. The buffering of Ca^{2+} will reduce the peak Ca^{2+} concentration in the cell body, but also slows down diffusion from the cell body to the rhabdomere and consequently slows down extrusion of Ca^{2+} by the Na^{+}/Ca^{2+} exchanger, which is in agreement, both with previously reported cell body Ca^{2+} concentration levels measured with Ca^{2+} dyes (18, 23) and the measured tail currents (this study).

Supporting References

1. Gerster, U. 1997. A quantitative estimate of flash-induced Ca^{2+}- and Na^{+}-influx and Na^{+}/Ca^{2+}-exchange in blowfly *Calliphora* photoreceptors. Vision Res. 37:2477-2485.
2. Postma, M., J. Oberwinkler, and D. G. Stavenga. 1999. Does Ca^{2+} reach millimolar concentrations after single photon absorption in *Drosophila* photoreceptor microvilli? Biophys. J. 77:1811-1823.
3. Oberwinkler, J., and D. G. Stavenga. 2000. Calcium imaging demonstrates colocalization of calcium influx and extrusion in fly photoreceptors. Proc. Natl. Acad. Sci. USA 97:8578-8583.
4. Suzuki, E., E. Katayama, and K. Hirosawa. 1993. Structure of photoreceptive membranes of Drosophila compound eyes as studied by quick-freezing electron microscopy. J. Electron Microsc. 42:178-184.
5. Reuss, H., M. H. Mojet, S. Chyb, and R. C. Hardie. 1997. In vivo analysis of the *Drosophila* light-sensitive channels, TRP and TRPL. Neuron 19:1249-1259.
6. Liu, C. H., T. Wang, M. Postma, A. G. Obukhov, C. Montell, and R. C. Hardie. 2007. In vivo identification and manipulation of the Ca^{2+} selectivity filter in the *Drosophila* Transient Receptor Potential Channel. J. Neurosci. 27:604-615.
7. Blaustein, M. P., and W. J. Lederer. 1999. Sodium calcium exchange: Its physiological implications. Physiol. Rev. 79:763-854.
8. Weber, C. R., K. S. Ginsburg, K. D. Philipson, T. R. Shannon, and D. M. Bers. 2001. Allosteric regulation of Na/Ca exchange current by cytosolic Ca in intact cardiac myocytes. J. Gen. Physiol. 117:119-131.
9. Hardie, R. C. 1995. Photolysis of caged Ca^{2+} facilitates and inactivates but does not directly excite light-sensitive channels in *Drosophila* photoreceptors. J. Neurosci. 15:889-902.
10. Gu, Y., J. Oberwinkler, M. Postma, and R. C. Hardie. 2005. Mechanisms of light adaptation in *Drosophila* photoreceptors. Curr. Biol. 15:1228-1234.
11. Kushmerick, M. J., and R. J. Podolsky. 1969. Ionic mobility in muscle cells. Science 166:1297-1298.
12. Allbritton, N. L., T. Meyer, and L. Stryer. 1992. Range of messenger action of calcium ion and inositol 1,4,5-trisphosphate. Science 258:1812-1815.
13. Li, Y., and S. Gregory. 1974. Diffusion of ions in sea water and in deep-sea sediments Geochim. Cosmochim. Acta 38:703-714.
14. Porter, J. A., M. Yu, S. K. Doberstein, T. D. Pollard, and C. Montell. 1993. Dependence of calmodulin localization in the retina on the NINAC unconventional myosin. Science 262:1038-1042.
15. Ballinger, D. G., N. Xue, and K. D. Harshman. 1993. A Drosophila photoreceptor cell-specific protein, calphotin, binds calcium and contains a leucine zipper. Proc. Natl. Acad. Sci. USA 90:1536-1540.
16. Martin, J. H., S. Benzer, M. Rudnicka, and C. A. Miller. 1993. Calphotin: a Drosophila photoreceptor cell calcium-binding protein. Proc. Natl. Acad. Sci. USA 90:1531-1535.
17. Weiss, S., E. Kohn, D. Dadon, B. Katz, M. Peters, M. Lebendiker, M. Kosloff, N. J. Colley, and B. Minke. 2012. Compartmentalization and Ca^{2+} Buffering Are Essential for Prevention of Light-Induced Retinal Degeneration. J. Neurosci. 32:14696-14708.
18. Rosenbaum, E. E., R. C. Hardie, and N. J. Colley. 2006. Calnexin is essential for rhodopsin maturation, Ca^{2+} regulation, and photoreceptor cell survival. Neuron 49:229-241.

19. Maune, J. F., C. B. Klee, and K. Beckingham. 1992. Ca2+ binding and conformational change in two series of point mutations to the individual Ca^{2+}-binding sites of calmodulin. J. Biol. Chem. 267:5286-5295.
20. Paulsen, R., D. Zinkler, and M. Delmelle. 1983. Architecture and dynamics of microvillar photoreceptor membranes of a cephalopod. Exp. Eye Res. 36:47-56.
21. Zinkler, D., J. Bentrop, and R. Paulsen. 1985. Phospholipids of fly photoreceptor membrane : fatty acid and phosphoinositide metabolism. Verh. Dtsch. Zool. Ges. 78:303.
22. McLaughlin, S., and J. E. Brown. 1981. Diffusion of calcium in retinal rods. A theoretical calculation. J. Gen. Physiol. 77:475-487.
23. Hardie, R. C. 1996. INDO-1 measurements of absolute resting and light-induced Ca^{2+} concentration in *Drosophila* photoreceptors. J. Neurosci. 16:2924-2933.
24. Oberwinkler, J. 2002. Calcium homeostasis in fly photoreceptor cells. Adv. Exp. Med. Biol. 514:539-583.
25. Mojet, M. H., J. Tinbergen, and D. G. Stavenga. 1992. Receptor potential and light-induced mitochondrial activation in blowfly photoreceptor mutants. J. Comp. Physiol. A 168:305-312.
26. Peretz, A., C. Sandler, K. Kirschfeld, R. C. Hardie, and B. Minke. 1994. Genetic dissection of light-induced Ca^{2+} influx into *Drosophila* photoreceptors. J. Gen. Physiol. 104:1057-1077.